University of Alberta

Prospective structured support and nanostructured active phase for oil upgrading

by

Arvind Chhabra

A thesis submitted to the Faculty of Graduate Studies and Research
in partial fulfillment of the requirements for the degree of

Master of Science
in
Chemical Engineering

Department of Chemical and Materials Engineering

Abstract

Selective ring opening of naphthenic compounds is a preferred reaction to increase cetane number of fuels. Indan ring opening was studied using both structured and powdered catalysts. A structured support of Sintered Metal Fibers (SMF) filter materials (FeCrAl alloy) was surface-oxidized to form α-alumina whiskers. Practical conversions were achieved with Ir nanoparticles preformed in the presence of polyvinylpyrrolidone stabilizer. The SMF unique structure was found to eliminate mass and heat transfer limitations. Due to the low surface area of SMF, Ir nanoparticle agglomeration was observed. Temperature effects on the product yield and conversion were evaluated. The catalyst thermal pretreatment was shown to remove 81% of the Ir organic stabilizer. The study may pave the way to the development of structured catalysts with enhanced mass and heat transfer limitations for fast catalytic reactions requiring low loading of catalytically active phase.

Acknowledgments

I would like to thank my supervisor Dr. Natalia Semagina and my co-supervisor

Dr. John A. Nychka for their kind guidance through my studies.

Special Thanks to our group members Hessam Ziaeiazad, Jing Shen and Long Wu

for their support and help.

Contents

LIST OF TABLES

LIST OF FIGURES

LIST OF SYMBOLS, NOMENCLATURE AND ABBREVIATIONS

Symbol, Nomenclature or Abbreviation	Description
SMF	Sintered Metal Fibers
Ni	Nickel
Mo	Molybdenum
Ir	Iridium
Ox-SMF	Oxidized SMF
TEM	Transmission Electron Microscopy
RO	Ring Opening
Fe	Iron
Cr	Chromium
Al	Aluminum
DCM	Di-Chloro Methane
AAS	Atomic Absorption Spectroscopy
SEM	Scanning Electron Microscopy
AES	Auger Electron Spectroscopy
TGA	Thermo Gravimetric Analysis
HDS	Hydro Desulfurization
EPA	Environmental Protection Agency
Co	Cobalt
CSTR	Continuous Stirred Tank Reactor
PFR	Plug Flow Reactor
PBR	Packed Bed Reactor
L	Concentration of active sites
η	Effectiveness factor
k	Rate constant [$mol^{1-n} \cdot L^{n-1} \cdot s^{-1}$]
R	Rate of the reaction [mol/g.s]
$f_{(C)}$	A function of concentrations
ϕ^p	Thiele modulus
D_e	Diffusivity [m^2/s]
Pt	Platinum
Wt.%	Weight percent
CNF	Carbon Nano Fibers
ACF	Activated Carbon Fibers
MBE	2-methyl-3-buten-2-ol
PVP	Poly Vinyl Pyrrolidone
GC	Gas Chromatography
FID	Flame Ionization Detector

NAA	Neutron Activation Analysis
MTL	Mass Transfer Limitation
HTL	Heat Transfer Limitation
C_{WP}	The Weisz-Prater number
ϕ_1^2	The ratio of evaluated reaction rate to diffusion rate (squared)
$-r_A$	Rate of consumption of A [mol/g.s]
ρ_c	Catalyst density [kg/ m^3]
C_{As}	Surface concentration
ε	Porosity
δ	Constrictivity
τ	Tortuosity
$d(t)$	Catalyst decay
FTIR	Fourier transform infrared spectroscopy
T	Temperature
A	Arrhenius factor [$mol^{1-n} \cdot L^{n-1} \cdot s^{-1}$]
E_a	Activation energy (observed) [kJ/mol]
R_g	Universal gas constant [J/mol.K]

Chapter 1. Introduction

Decrease in the quality of crude oil has forced the industry to use more severe conditions in oil upgrading reactors. As the process severity increases, mass and heat transfer characteristics of the used catalysts are becoming of paramount importance. This leads to the quest of catalysts with highly active and selective active phase with a support allowing the absence of mass and heat transfer limitations. A type of catalyst with metal structured support can be a good answer to this demand due to its higher heat conductivity and uniform flow distribution; however, the loading and adherence of active phase on this kind of low surface area support can be a problem. The utilization of a structured support for a specific operation, which is a part of the goal of this study, requires preparation of an efficient structured catalyst with optimum loadings to avoid large reactor sizes.
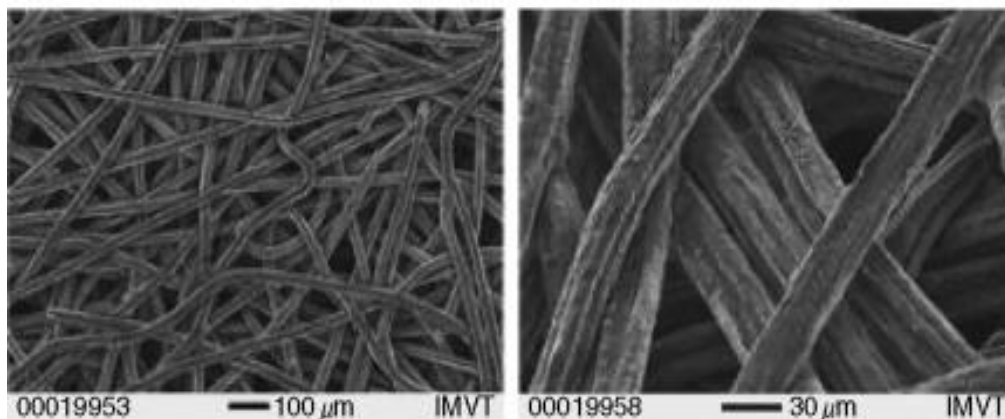
Fig.1. SEM images of SMF

The proposed support in this study is Sintered Metal Fibers (SMF) filters made of FeCrAl alloy which looks like a 3-D net under a microscope (Fig. 1).

SMF falls under the category of structured (arranged) catalysts. Arranged catalysts have the benefit of lower pressure drop due high porosity (~ 80%) with channels located between the microfibers in the 3-D net structure (Fig. 1), they also act as static mixers. Since the support is organized, the simulation and design can be done easier than for other types of catalysts. This type of catalyst has been proven to provide an effective environment for mass and heat transfer [1]. It was previously shown that SMF eliminates mass transfer limitations in three phase hydrogenation [2] so this support was chosen for further studies. An advantage of the SMF material is its ability to form alumina whiskers upon thermal oxidation, which can be used for active phase deposition.

The main goal of this study is to develop SMF as a structured catalyst support and/or nanostructured iridium particles as active metal for indan ring opening, which is a model reaction in oil upgrading. The oxidized SMF used as catalyst support was first developed via thermal oxidation by Jadid E. Samad [2]. It contains α - and θ - alumina whiskers of 200 nm on its fibers, which provides a higher surface area and a good opportunity to deposit active metal. The first challenge of utilizing of SMF is to find a precursor that could be deposited to perform indan ring opening. As the first step, we aim to deposit Ni and Mo on

the support as they are widely used in hydrotreatment, including in the presence of sulfur, and are less expensive compared to noble metals; as an alternative, Ir nanoparticles with known ring opening activity will be used as the active phase. Due to the hydrophobicity of oxidized SMF [2], the tested precursors are organic nickel precursor (bis-cyclopentadienyl-nickel) in toluene, organic molybdenum precursor (bis-acetylacetonato-dioxomolybdenum VI) in DCM (Di-Chloro Methane) and preformed Ir nanoparticles in ethanol. AAS (Atomic Absorption Spectroscopy) and SEM/AES (Scanning Electron Microscopy/Auger Electron Spectroscopy) are used to understand the dispersion and deposition of active phase on SMF. The ring opening reaction is to be verified for the absence of mass and heat transfer limitations. An optimal reaction temperature to achieve higher desired product yield will be found.

Since preformed metal nanoparticles are less likely to sinter when deposited on the support (and this was the main problem of Ni deposition on SMF), so they were chosen for further study using SMF as support. In this research, Polyvinylpyrrolidone (PVP) was used to produce preformed Ir nanoparticles. The catalyst preparation method was called alcohol reduction method during which alcohol was used to reduce the Ir to its metallic form and PVP was used to stabilize the Ir particles and prevent them from agglomeration (size control) due to the fact that small nanoparticles (~10nm) was needed in order to have large surface area (which leads to higher catalytic activity). After the deposition of

such nanoparticles on the catalyst support, PVP and other remaining organic materials (remaining of Ir organic solid precursor) are considered undesired due to the fact that they prevent the surface of the active sites to be accessible by the reactants, thus a thermal step called calcination was performed to remove such organic undesired materials from the catalyst.

Towards the fulfillment of the main goal of this thesis, which is the utilizing of SMF for RO reaction and investigating the RO reaction using Ir nanoparticles and the factors involved in catalyst preparation, the Thermo Gravimetric Analysis (TGA) was used to investigate the removal of Ir nanoparticle stabilizer (PVP) and other organic remaining whose presence in reaction could affect the active phase performance. A procedure during which organic materials will be removed by 81% was used as the calcination step towards catalyst preparation for RO reaction performed in this study.

Chapter 2. Literature review

2.1. Catalysis in oil upgrading

Oil upgrading is a cumulative term for a wide variety of processes from hydrotreatment to thermal and metal separation processes. These processes are mostly applied to heavy fractions of crude oil in order to make them lighter and cleaner for different purposes such as improving cetane number (for diesel fuels), improving octane number (for gasoline production), removing sulfur and nitrogen (to meet the environmentally forced regulations). Such structural changes in hydrocarbons occur only via chemical reactions, mainly hydrogenolysis. The majority of these structural changes need catalyst in order to increase the rate of the reaction and desired product yield. Catalysts can get deactivated; hence the choice of a suitable catalyst for a reaction requires knowledge of the chemical reaction and properties of the materials involved. The choice of the active, selective and stable catalyst plays a vital role in hydroprocesses; for the processes to be cost effective, the costs of providing hydrogen and high pressure equipment should be also optimized. Having all of the mentioned factors in mind, one can understand that using a certain catalyst (such as Ni or Ir) in a certain reaction (such as ring opening or hydrogenation) requires a knowledge which can be achieved by investigating both catalyst and reaction behaviour.

2.1.1. Hydrodesulfurization

Recently, Hydrodesulfurization (HDS) has received increased attention due to environmentally forced regulations such as Directive of the European Parliament [4] and the Environmental Protection Agency (EPA) Clean Air Act (Tier 2) [5]. In order to achieve a more environmentally clean fuel, 10-15 billion dollars in Europe and 16 billion dollars in the USA and Canada will be spent as a response to new regulations [6, 7]. Since every crude oil contains sulfur, hydrodesulfurization is always needed to improve the oil quality. Lower boiling point cuts have sulfur as mercaptans and cyclic sulfides. Higher boiling point cuts have sulfur as polycyclic compounds. Higher boiling point cuts of crude oil contain more sulfur [14].

Table.1. Sulfur content in different crudes [12]

	S% in Crudes	Distribution of S in various fractions			
		Gasoline+Naphta	Kerosene	Gas oil	Heavier components
Middle East	0.15	0.3	3.6	38.6	57.5
Texas	0.36	0.9	1.3	15.4	82.4
Iran	1.40	1.1	1.5	12.6	84.8
West Texas	2.00	1.8	4.2	14.8	79.2
Kuwait	2.45	0.1	0.8	9.5	89.6

Ma et al. [8] categorized the sulfur compounds of diesel fuel into 4 categories:

1) Alkyl benzothiophenes

2) Dibenzothiophenes and alkyl dibenzothiophenes without substituents on 4 and 6 positions

3) Alkyl dibenzothiophenes with only one substituents at 4 or 6 position

4) Alkyl dibenzothiophenes with multiple substituents at 4 and 6 positions

As it goes from 1 to 4, the desulfurization gets more difficult. The rate constant for hydrodesulfurization of second group was reported to be 0.034-0.100 min^{-1} while this constant for third and fourth group was reported 0.013-0.034 min^{-1} and 0.005-0.013 min^{-1} respectively [8].

In the beginning of the history of hydrodesulfurization study, pulse micro reactors were used due to their simple structure [9]. For example, 5 mg of catalyst was loaded in a micro reactor and then heated up to 400°C under hydrogen flow followed by a pre-treatment using H_2S (10 mole%) for 2 hours (40 mL/min). Every 35 minutes, a pulse of reactants was introduced (0.5 μl) to the reactor until a constant conversion was achieved. Kilanowski et al. [9] found that in a pulse micro reactor, there is lack of dependency of reactivity on the number of reactant`s rings at low pressures while at high pressures, the reactivity decreases by increasing the number of rings in reactant. Batch reactors were also common [10] at pressures around 10 MPa. Ledoux et al. [11] showed that with the help of carefully applied kinetics and having this in mind that catalysts

of different families (Co and Mo, Ni and Mo) should not be mixed; the HDS of thiophene at atmospheric pressure is a suitable model to predict the HDS of dibenzothiophene at industrial pressure. In order to get close to industrial conditions, a high pressure flow micro reactor was introduced by Eliezer et al. [12, 13] in which the reactor packing was alumina and had a volume of 0.325 cm^3 and the pressure went up to 300 atm. The reported results indicated that dibenzothiophene and 4-methyldibenzothiophene had similar reaction networks leading to producing biphenyl and its subsequent hydrogenation.

2.1.2. Hydrodesulfurization classification

HDS processes can be classified as (a) decomposition of sulfur compounds, (b) separation of sulfur compounds and (c) separation followed by decomposition of sulfur compounds [15]. Conventional HDS processes fall under the first category, during which the sulfur compounds decompose and convert to gaseous or solid sulfur plus recovered hydrocarbons without sulfur. In the second type processes, the sulfur parts of the stream are separated and if they cannot be separated easily, they are decomposed to molecules that are easier to separate. In this kind of process, some hydrocarbons can be separated along with sulfur compounds and this is not in favour of the refinery objectives due to the fact that the refinery is losing some hydrocarbons. Desulfurization by catalytic distillation falls under the third category: separation and decomposition occur at the same time and in the same unit that is a desirable combination of processes and can result

in efficient sulfur removal. This process allows to have a hydrodesulfurization unit in its compact form (instead of two units for separation and decomposition) and also the refinery does not lose any desired hydrocarbons.

In conventional HDS processes, the sulfur compounds convert to H_2S and sulfur-free hydrocarbons. This is done with the help of catalysts, such as $CoMo/Al_2O_3$ and $NiMo/Al_2O_3$. For deep HDS, more severe conditions are needed but high pressures and temperatures lead to undesired side reactions and products. Therefore, modifying the catalyst activity and selectivity is a more promising way of deep HDS, which has been achieved so far such as CoMo and NiMo STARS (Super Type II Active Reaction Sites) which was introduced by Akzo Nobel [15]. The next step towards improving these processes was to switch from co-current reactors to counter-current reactors. For example SynSat Technologies [16, 17], which uses both co-current and counter-current processes to achieve a proper efficiency.
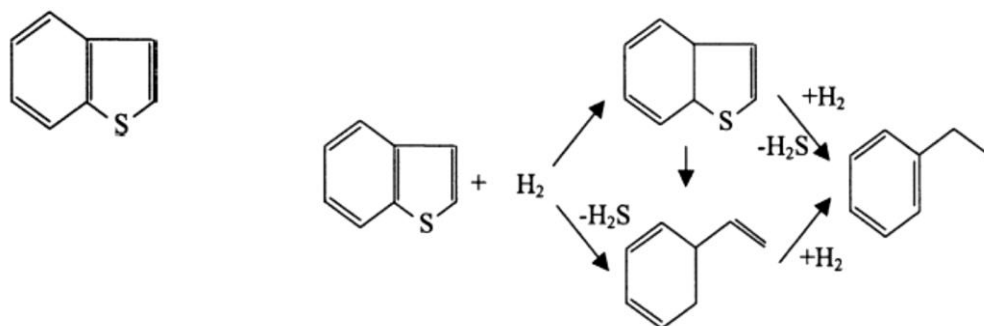
Fig.2. Benzothiophene pathways of desulfurization, reprinted from [15] with permission from Elsevier

2.1.3. Reactors in oil upgrading

There are two types of reactors, which are used in oil upgrading [5]: a) Batch, b) Continuous reactors.

2.1.3.1. Batch reactors

The applications of batch reactors are mainly limited to small scale operations, such as testing processes which are recently being developed and have not yet been fully developed, production of expensive materials and generally the processes that are not suitable for continuous operation. The benefit of batch reactors is having high conversions, which can be achieved by high contact time of reactants in the reactor. The reactor disadvantages are high labor costs per batch, the variability of products between batches and large scale production difficulties [65].

Batch reactors range in size from a few millilitres to a few litres. The use of stirring and baffles is intended to improve turbulence which leads to better contact of catalyst and feed (mostly asphaltene and metal containing feeds) in these systems. The ratio of the reactor diameter to catalyst particles is a factor which determines the role of the catalyst size in the reaction. In industry, the ratio of the reactor diameter to catalyst particles diameter is very high. Hence in order to duplicate laboratory conditions, reactors with high diameters should be

used. Smaller autoclaves lead to results, which are more dependent on catalyst size and formation (due to lower ratio of reactor diameter to catalyst particles diameter) so these kinds of reactors are suitable for investigating the overall catalyst behaviour and diffusion problems, which always exist in heavy oil upgrading. The main disadvantage of batch reactors is the trapping of H_2S or NH_3 in the reactor, which leads to lower ratio of H_2S/H_2 (resulting in poor maintenance of active sites) and poisoning of catalyst (NH_3 can act as a poison however it is a rather weak poison among Nitrogen compounds [18]). In the presence of both H_2S and NH_3 (or other Nitrogen compounds), it is believed that these two can react and form ammonium sulfide and amine sulfur particulates [19]. Considering all of the factors mentioned above, since the rate of the reaction in batch reactors is higher in the early stages, the data is less affected during the first stages of reaction than the data obtained from the reactor after early stages.

2.1.3.2. Continuous reactors for oil upgrading

2.1.3.2.1. Continuous Stirred Tank Reactor (CSTR)

This type of reactor is a stirred tank, which operates under continuous condition. CSTR is mainly used for liquid phase reactions and the flows are considered steady state. The tank`s contents are presumed to be thoroughly mixed; hence there will be no temperature or mass gradient in the tank. Due to the fact that

temperature and concentration are the same at every point of the tank, the outlet flow would have the same properties as the tank`s contents. In the reactors, which perfect mixing won`t be achieved, residence time distribution should be taken into consideration [65].

2.1.3.2.2. Tubular Reactor

The tubular reactor is a cylindrical reactor, which operates mostly under steady state condition. Tubular reactors are mainly used for gas phase reactions. The assumption which can describe the behaviour of this type of reactor is that there is no radial gradient of velocity, temperature or concentration so based on this assumption, the reactor operates in plug flow. This is the reason that these reactors are frequently being called Plug Flow Reactors (PFR). There is an axial concentration gradient in these systems through the length of the tubular reactor, which shows that there are less reactants and more products present, as we go from one axial point to another further one [65].

2.1.3.2.3. Packed Bed Reactor (PBR)

This type of reactor usually has a bundle of tubes, in which there are pellets of catalyst and is generally used for heterogeneous catalyzed reactions. The active catalyst surface area plays a significant role in the rate of reaction. Transport processes which should be taken into consideration for a PBR have a variety of aspects, such as axial and radial gradients of concentration and temperature and

gradients within the pellets; hence the complexity of PBR is beyond a simple model [66].

In PBR reactors, the products are constantly removed from the reactor hence the effects of hydrodesulfurization and hydrodenitrogenation products (such as H_2S and NH_3) will be less on catalyst and due to continuous introduction of hydrogen to the system, the ratio of H_2 to H_2S or other compounds can be maintained in favour of the desired products. As an example, Gualda and Kasztelan [20] saw different deactivation trends in batch reactors and continuous reactors (which were similar in other ways).

2.1.4. Mass and heat transfer limitations and tests

The data, which is achieved for kinetic studies should be free of mass transfer and heat transfer effects therefore concentration and temperature gradients should be removed from catalyst support (intra particle gradients) and between surfaces and phases (inter phase gradients). Some of the ways, which have been reported to kinetic regime verification, had problems such as not being general (cannot be used in a variety of situation and reactions) [21], not practical (the technique depends on a factor which is difficult to measure) [22] or assumption of knowing the rate expression (which in most cases is not known) [23]. Madon and Boudart [24] suggested a way to investigate the presence of heat and/or mass transfer limitations, which did not have the problems stated above.

The limitations can occur due to having problems regarding calculation of values such as effective diffusivity, heat transfer coefficient, particle size. Regarding flow reactors, if the conversion remains constant by increasing the flow rate of reactants at a certain space velocity, then it can be said that the effect of external mass transfer on the results is negligible because by increasing the flow rate, we increase the Reynolds number and if that cannot effect the rate of reaction, so the mass transfer factor is not involved in the rate of reaction. As for slurry reactors, the increase in Reynolds number can be done by increasing agitation and if constant conversion is seen then there will be no external mass transfer limitations. The mentioned test may not be accurate when the system is working under laminar condition (low Reynolds numbers) and also it does not show if the results are free of internal mass transfer limitations or not. The test, which is explained in the following paragraphs does not have the problems mentioned and were first suggested by Koros and Nowak [25] and then developed by Madon and Boudart [24].

The test is based on changing the concentration of active material on the catalyst support. The effectiveness factor in a kinetic control reaction is 1 ($\eta=1$). The rate constant (k) depends on the concentration of active sites (L) and in the presence of severe internal diffusion limitations, the rate constant will be proportional to $L^{1/2}$ and if there is severe external mass transfer limitations, the rate constant will be independent of L [26, 24], the rate constant with no mass transfer

limitations can be defined as a function of loading and the constant for using pure catalyst:

$$k = L \cdot k_0 \qquad \text{(Eq.1)}$$

k_0 is the rate constant in a system with L=1. The concentration of active sites can be expressed with respect to surface area or grams of catalyst (wt.% or per unit surface of catalyst). There should be an effectiveness factor in the rate equation due to the fact that the rate of reaction may be controlled by mass transfer factors.

$$R = \eta R_0 = \eta \cdot L \cdot k_0 \cdot f_{(C)} \qquad \text{(Eq.2)}$$

Where R_0 is the rate without any mass transfer limitations and $f_{(C)}$ is the function of concentrations, which are involved in the reaction rate. The effectiveness factor can be expressed (quantitatively) as Thiele modulus ($\eta = \phi^p$), which is proportional to $L^{p/2}$.

$$R = \phi^p \cdot L \cdot k_0 \cdot f_{(C)} \qquad \text{(Eq.3)}$$

$$R \propto L^{(1+p/2)} = L^s \qquad \text{(Eq.4)}$$

Thiele modulus is a dimensionless number, which shows the ratio of reaction rate to mass transfer rate. The Thiele modulus is defined in a way that its square shows the ratio of $1/(k_0.C_0^{n-1})$ (which is a characteristic time for reaction) to R^2/D_e (which is a characteristic time for diffusivity). When there are no mass transfer limitations, the modulus is a very big number because the mass transfer characteristic time is much less than the reaction characteristic time (the diffusion rate is higher than reaction rate) and when there are limitations, the modulus becomes small [27].

If there is no mass transfer limitations, then the effect of mass transfer is zero therefore the effectiveness factor which is included in the equation mainly because of mass transfer factors should become one ($\eta=1$) so p=0 and s=1. In case of severe mass transfer limitations, "p" should be an amount to have an effectiveness factor depending directly on radius of particles (R) or diffusivity (D_e). In severe internal mass transfer limitations, this dependence should be a function of D_e and root square of particles radius (R) so the "p" should be -1 (so s=1/2) and η will be very small so s would be ½. In cases of severe external mass transfer limitations, the loading should have no effect on the rate equation (since increasing and decreasing the loading would give an equal conversion) so "s" should be zero and consequently, p=-2. Also if s=1 is achieved at 2 different temperatures, the system works under isothermal condition (absence of any

temperature gradients). In order to know the value of s, the graph of Ln (rate) versus Ln (loading) should be drawn and the slope of the graph shows "s".

2.1.5. Ring opening

Ring opening of cyclic (or polycyclic) hydrocarbons is a common way of improving the fuel quality (cetane number, desulfurization, denitrogenation). Polycyclic aromatics and naphtene hydrocarbons are undesirable in diesel fuels due to their condensations on catalysts, coke particulate formation in exhaust gases and low cetane numbers. Ring opening is usually studied using model compounds (aromatics, sulfur containing molecules, nitrogen containing molecules) to evaluate various ring opening pathways.

The three pathways of ring opening are free radical, acid-catalyzed carbocation and metal catalyzed hydrogenolysis. In free radical pathway, the RO is achieved via pyrolysis which makes it very difficult to have high yields of ring opening since competitive secondary reactions limit the reaction yield. In acid-catalyzed carbocation, since the reaction is controlled by acid function, excessive cracking of side chains occurs. During metal catalyzed hydrogenolysis, both endocyclic and exocyclic carbon bonds can be broken but in order to achieve a selective ring opening (i.e. opening naphthenic ring without loss of molecular weight), only endocyclic bond breaking is preferred. Gault et al. [81] categorized RO mechanisms into three categories: dicarbene, π-adsorbed olefin and

metallocyclobutane. Dicarbene mechanism resulted in cleavage of unsubstituted carbon bonds leading to the production of branched isoparaffins (low cetane number). The two other mechanisms (i.e. π-adsorbed olefin and metallocyclobutane) led to cleavage of carbon bonds at substituted position resulting in production of products with high cetane numbers; hence these two mechanisms are preferred. Typically, the dicarbene mechanism is preferred when using Ir as active phase [82].

In this thesis, iridium was used as a noble metal catalyst with high activity and indan was used as a model compound for ring opening and hydrodesulfurization (a model for Benzothiophenes) so there is a special emphasis in this section on noble metal catalysis for indan and Benzothiophene.

Nylen et al. [28] have done some studies on ring opening of indan over Pt-Ir based catalysts and have investigated the effect of catalyst support and combination on ring opening. Seven different materials were used as support for a combination of Pt-Ir catalyst (2 wt% Pt_5Ir_{95}) and the depositions were done via incipient wetness impregnation method. These catalysts were tested for ring opening of indan in hydrogen (gas phase) at atmospheric pressure. Also the most effective support (based on [28], CeO_2) was used to investigate the effect of Pt-Ir combination.

In RO of indan, the two desired products are 2-ethyltoluene and n-propylbenzene due to their high octane and cetane numbers (respectively). α ring opening leads to production of n-propylbenzene (cetane number improvement) and β ring opening results in production of 2-ethyltoluene (octane number improvement) (Fig.3). β ring opening is preferred in indan ring opening due to bond dissociation energy (BDE) difference (BDE of C_6H_5-C_2H_5 is 99kcal/mol, BDE of C_6H_5 CH_2-CH_2 is 73 kcal/mol) [83].
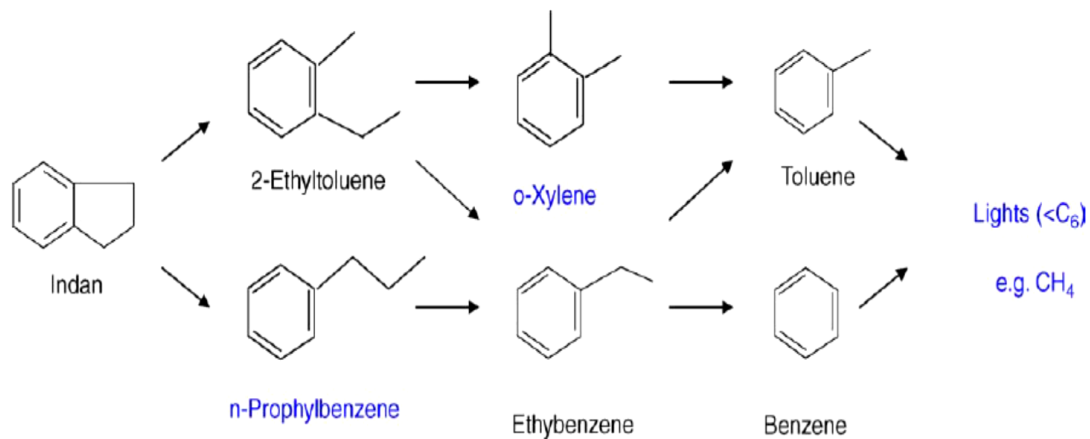
Fig.3. Indan ring opening pathways, reprinted from [28] with permission from Elsevier

The activity of catalysts on various supports is shown in Fig.4.
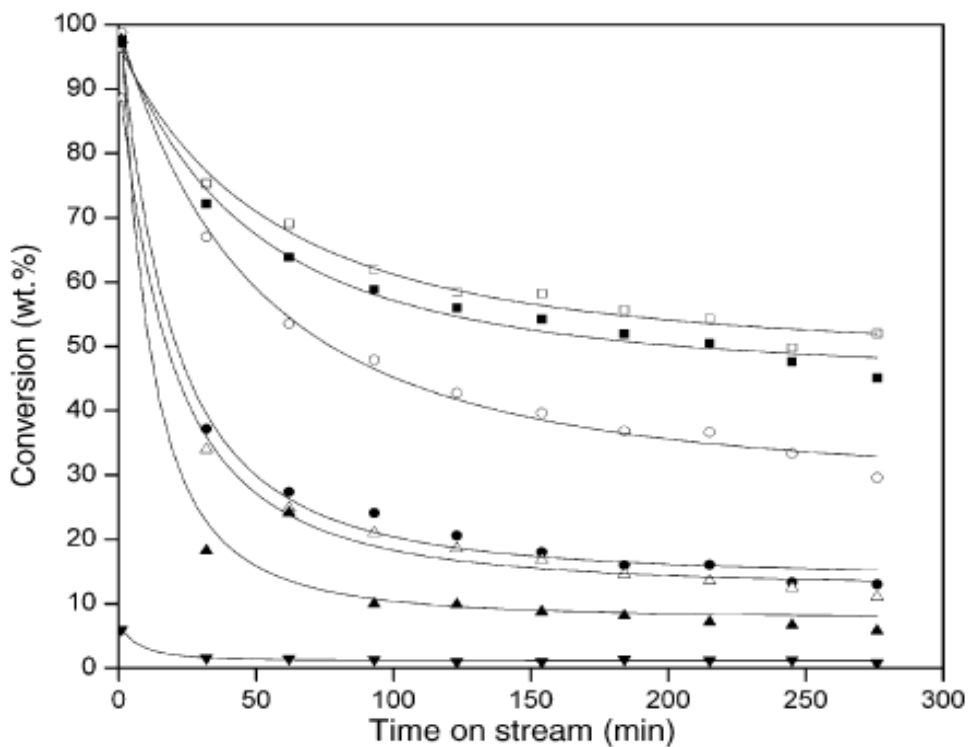
Fig.4. Conversions of indan ring opening at 325°C and atmospheric pressure over 2 wt% of Pt_5Ir_{95} catalysts on (from top to bottom): CeO_2, γ-Al_2O_3, SiO_2-Al_2O_3, H-SA, ZrO_2, MgO and SiO_2 versus Time on Stream (min), reprinted from [28] with permission from Elsevier

The best catalyst support was found to be CeO_2 so this support was used to investigate the effect of Pt-Ir combination ratios. It was clearly seen that pure Ir as active metal had the highest conversion and Pt as active metal had the lowest conversion.
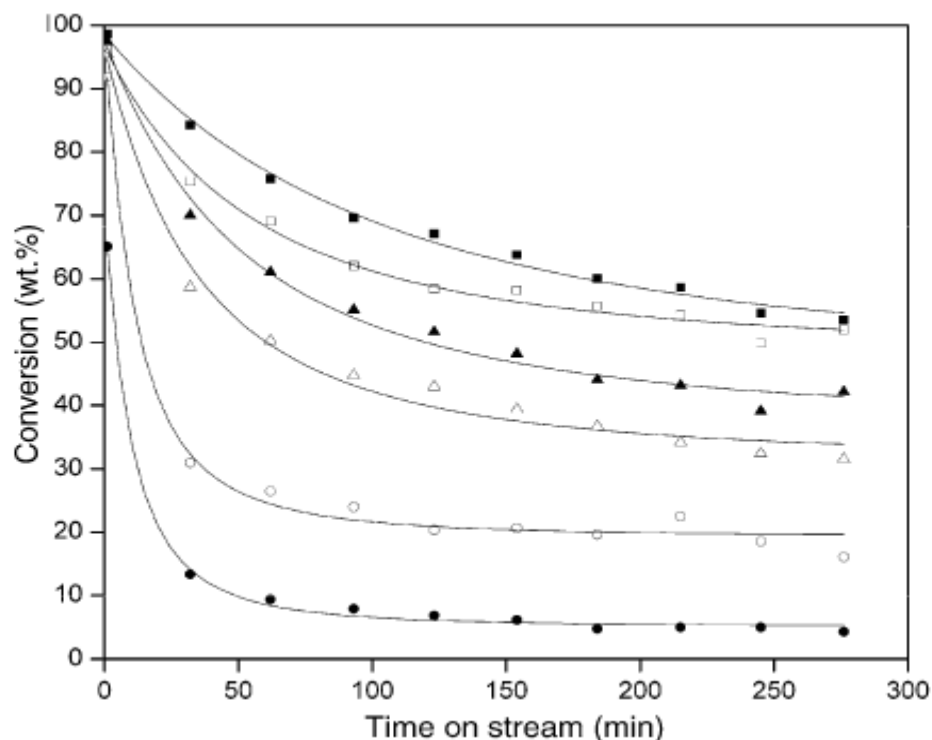
Fig.5. Conversions of indan ring opening over different 2 wt% catalysts on CeO_2 (from top to bottom): Ir, Pt_5Ir_{95}, $Pt_{15}Ir_{85}$, $Pt_{25}Ir_{75}$, $Pt_{50}Ir_{50}$ and Pt versus Time on Stream (min) , reprinted from [28] with permission from Elsevier

Nylen et al. in other research [29] have investigated the effect of pressure on indan ring opening using Pt-Ir bimetallic catalyst on boehmite. 2 wt% Pt-Ir/boehmite was proved to be a good bi-metallic catalyst, which performs better than the corresponding Pt/boehmite catalyst regarding indan ring opening. TEM showed agglomeration of platinum clusters over iridium platelets [28]. This catalyst under low pressure (atmospheric pressure) resulted in selective ring opening while under high pressure (40 bars), it led to hydrogenation.

The reaction conditions were: pretreatment (reduction) was programmed to reach 450°C with a rate of 4°C/min and held at 450°C for 1 hour under a hydrogen rate of 100 cm^3/min, the indan flow was 0.4 cm^3/h and the reactor was

a fixed bed catalytic reactor with pellets of catalyst in it. These conditions were the closest one to this thesis conditions (375°C for pretreatment and 350°C for reaction at 50-120 mL/min hydrogen flow).

Davidova et al. [30] has reported that the primary product of indan ring opening over Ni/Al$_2$O$_3$ was 2-ethyltoluene but it further dealkylates to o-xylene, ethylbenzene, toluene and benzene while n-propylbenzene was not a product at atmospheric pressure.

Guidot and Germain [31] have reported that in liquid phase below 400°C using Ni and Co at 80 to 195 atm, the pressure role in reaction rates of hydrogenation and hydrogenolysis was negligible.

Ring opening of model compounds with the help of noble metals as catalyst (which are very selective in ring opening), is known to have some problems with the real sulfur containing feeds. These noble metals are very sensitive to sulfur and easily get poisoned by sulfur containing compounds. The main reason of poisoning is the production of H$_2$S during the hydrodesulfurization. H$_2$S gets adsorbed by metal sites and this leads to less interaction between metal and support resulting in agglomeration and particle size growth of active metal [33]. The sulfur tolerance of active metals can increase with enhancing the metal-support interaction.

Frety et al. [32] investigated the effect of support on catalyst resistance towards sulfur. 3 iridium based catalysts on different supports were prepared and tested in a sulfur containing reaction. The three different supports were MgO, Al_2O_3 and SiO_2-Al_2O_3. iridium loading on each support was 0.5 wt% and each catalyst was pretreated under hydrogen flow rate of 3.6 L/h at 500 °C for 5 hours. The reaction was done in a micro reactor using 0.01 g of each catalyst. The reference activity was tested using hydrogen and cyclohexane without any sulfur content and the poisoned activity was tested using a 3 ppm thiophene mixture in cyclohexane and a reaction time of 15 minutes. The pressure ratio of hydrogen to hydrocarbon was 14 and the reactions were done at 543 K. The ratios of poisoned activity to reference activity were 0, 0.015 and 0.2 for MgO, Al_2O_3 and SiO_2-Al_2O_3 respectively. On the other hand, the activity of each catalyst was tested separately in a reaction with dibenzothiophene at 270°C using 0.03 g of catalyst and ratio of H_2 to hydrocarbon of $1.5x10^5$. The activities were reported by the rate of dibenzothiophene removal and were 14, 12 and 5.5 for MgO, Al_2O_3 and SiO_2-Al_2O_3 respectively.

2.2. Structured catalysts and reactors

Conventional fixed bed catalytic reactors were the first choice in the past for structured reactors but this type of reactor has some problems. Maldistributions (leading to limiting the accessible catalytic surface area), high pressure drop and fouling sensitivity are some examples of the drawbacks of this kind of reactor.

Designing, simulation and scaling up a fixed bed reactor is very difficult due to random nature and characteristic of the reactor. An example of this confusing situation is catalyst particle size, which from a catalytic point of view should be smaller and from a pressure drop aspect of view should not be small. The disadvantages of conventional fixed bed reactors (mentioned above) motivated researchers to find other types of structured catalysts: Monolithic, Membrane and Arranged catalysts [5].

2.2.1. Monolithic catalysts

Uniform channels (parallel or zigzag) of metal or ceramic with different diameters can be used as a catalyst support. The channels` walls can be porous and used for deposition of active catalysts. In the case that the walls are not porous, the catalyst can be deposited on a porous material and then deposited on the walls. The former mentioned catalysts are called "incorporated monolithic catalysts" and the latter type of catalysts are called "washcoated monolithic catalysts" [1]. The name "Monolith" comes from a Greek word "mono lithos" meaning "composed of one rock" [34].

These types of reactors have some advantages such as low pressure drop, high surface area, proper distribution, no filter is needed and safer operation and the main setback about these reactors is the lack of knowledge in large scale processes [35].

Smits et al. [36] used a monolithic reactor for three phase hydrogenation. The feed stock was a mixture of styrene and 1-octane in toluene. The monoliths were cordierite channels washcoated with alumina followed by a deposition of Pd as active metal. The temperature range of the reaction was 43-80°C and the pressure range was 0.5-1.5 MPa. The liquid to gas ratio and linear velocity ranges were 1:1-6:1 m^3/m^3 and 0.05-0.45 m/s respectively. Hydrogenation was the dominant reaction for styrene and the major product was ethylbenzene on the other hand, isomerization was the prevailing reaction for 1-octane. Maldistribution of liquid (non-uniform wetting) can limit the reaction rate particularly at low liquid loadings.

Monolithic reactors are widely used as exhaust gas cleaners such as catalytic converters, diesel particulate filters and NO_x absorbers. NO_x absorbers monolithic reactors are washcoated containing barium, potassium or any other alkali/alkaline earth metal oxides [37, 38, and 39].

2.2.2. Membrane catalysts

If the wall of a monolith is permeable, then it will be called "wall-flow monolithic catalyst" or "membrane catalyst" so the active materials can be on or inside of the walls. The mass flow through the wall is very small due to the fact that this flow only occurs by diffusion. Diffusion limitations can occur in a case where a

current of flow is forced by an external factor (other than diffusion) through the walls.

Membrane technology started with desalinations and separation processes and then expanded to biotechnology, environmental and natural gas-oil processes. The main limiting factor for using membranes is that they are not readily available and the next factors are acceptable permeability, permselectivity and stability. The membranes are multifunctional due to their ability to separate and react [1]. With the help of separation aspect of membranes, reactions which are limited to low conversions due to thermodynamics can achieve higher conversions by removing the products selectively from reactor or introducing reactants to the reaction mixture. Membrane reactors can be classified as organic and inorganic membrane reactors. There is a more detailed classification mentioned by Tsotsi et al. [40].

One of the ways of reducing NO_x in coal gasification power plants is catalytic decomposition of ammonia. The decomposition of ammonia is an equilibrium limited reaction so it is a great opportunity to use membrane reactors to achieve high conversion. A comparative study of using membrane as a NO_x reducing process was performed by Collins and Way [41]. The study showed a 94% conversion over a palladium-ceramic membrane, which was a high conversion compared to conventional reactor, which showed 53% conversion. The reaction

conditions for both reactors was T=600°C and P=1618 kPa. The benefit of membrane usage was clearer for milder conditions (823 K) and the conversion was 79% for membrane while this value was 17% for conventional reactor.

2.2.3. Arranged catalysts

Arranged catalysts are placed perpendicular to the reactants flow, they have an open cross-flow structure characterized by intensive radial mixing. Catalysts which are arranged in arrays and packings covered with active material, fall under this category. Arranged catalyst is an effective solution for systems, which need intensive mass and heat transfer within the catalyst bed [1]. Structured catalysts have gained significant attention due to their low pressure drop and efficient heat and mass transfer. Pt metallic gauzes which are used in production of nitric acid are an industrial example of arranged catalysts [42].

Hydrogenation of sunflower oil over structured catalyst was investigated by Plourde et al. [43]. The effects of support pore volume and pore diameter were also investigated. The active metal used was Pd over structured silica and the loadings were between 0.7% and 5.0% (w/w).

Tribolet and Kiwi-Minsker [44] grew Carbon Nano-Fibers (CNF) on Sintered Metal Fibers (SMF) as a catalyst support for Palladium. They used this catalyst in

selective hydrogenation of acetylene and the activity of the catalyst was reported to be 10 times higher than Palladium on Activated Carbon Fibers (ACF).

Semagina et al. [45] used Sintered Metal Fibers (SMF) as a support for Pd and ZnO in a three phase hydrogenation reaction. The reactant was 2-methyl-3-butyn-2-ol (MBE) and the reaction temperature and pressure were 35°C and 5 bar respectively. The achieved yield was more than 95% and the observed catalyst activity was 10 times more than the industrial one (Pd, Pb/CaCO$_3$). The catalysts were regenerated with the help of ultrasonics and the selectivity and activity were almost like initial values.

Samad et al. [46] developed a new structured catalyst using Sintered Metal Fibers (SMF). SMF was thermally oxidized in three stages in order to grow alumina whiskers (200 nm height) on fibers and then Pd was deposited on the developed support and used in three phase hydrogenation of 2-methyl-3-buten-2-ol. The palladium nano particles which were deposited on SMF had a diameter of 20 nm and the loading on SMF was 0.5 wt%. This support was found to eliminate internal mass transfer limitations due to its unique pore structure and also pore mouth blockage didn't occur for this type of support. The thermal oxidation method which was presented in this paper was fast and simple compared to other methods presented before. This type of support (oxidized SMF) was used in some of this thesis experiments and has further been

investigated and studied in ring opening reaction using iridium nano particles as active phase.

2.3. Metal nanoparticles

Metal nano-materials have a wide range of applications such as electronics, optics, magnetic devices and catalysis. Physical and chemical properties of nano particles change with their size and shape so it is very important to have a method in order to have non-agglomerated and uniform distribution of particles. Chemical, physical and electrochemical methods have been studied to achieve a uniform size distribution of nano particles. Chemical methods are based on reduction of metal salts in solution [47], in microemulsion [48] or in sol-gel process [49]. The significant step in controlling the size of nano particles is nucleation and growth. The nucleation and growth step can be altered in many ways such as changing the activity of reducing reagent, changing the concentration of solution and changing the amount of surfactants or protective reagents [50]. From another point of view, we can prepare small metal nano particles and use them as centers for controlled nucleation and growth. The latter method is called seeding growth method, which has been used to synthesize nano particles of Au, Ag, Ir, Pd, and Pt [51-54].

 Chen et al. [55] used two different methods to achieve Ru nano particles. The first method was using ruthenium nitrosyl nitrate as salt and ethylene glycol as

reducing reagent followed by adding some PVP (Poly Vinyl Pyrrolidone) as a stabilizer, which led to achievement of controlled nano particle size of 1.2-6.5 nm with narrow size distribution. The second method was seeding growth method and by changing the seed to Ru^{3+} ratio, the particle sizes were controlled between 3.8 and 7.3 nm.

Yan et al. [56] investigated the effect of reducing agent (in this case, Ethylene Glycol, Diethylene glycol and Triethylene glycol) on nano particle size of Ru. The solutions were all polymer stabilized and were prepared by heating or refluxing a polyol solution. The average sizes of particles were controlled between 1.4 and 7.4 nm by changing the reducing agent, temperature or protective polymer. The standard deviation of size for any distribution achieved was less than 0.3 nm. As the reducing agent was stronger, the particle sizes were smaller due to faster reducing rate.

Teranishi and Miyake [57] could achieve nano particles of 17 to 30 Å by changing the amount of protective agent (PVP) and alcohol type/amount. They found that increasing the amount of protective agent would lead to smaller particles but they reported that this decrease in particles size had a limit dictated by alcohol type. The particle sizes which were obtained via different types of alcohol were in the order of methanol > ethanol > 1-propanol. This again illustrates the importance of reducing agent and reduction rate in synthesizing nano particles.

The smallest particle diameters were achieved in a solution of 40% alcohol by volume.

2.4. Alumina as a support

The most used metal oxide in the world is alumina, which has a variety of applications such as pump seals, electronic substrates, body armour, catalyst support. The key features which result in widespread use of alumina are [58]:

- High compressive strength

- High hardness

- Resistance to abrasion

- Resistance to most chemical attacks (even at high temperatures)

- High thermal conductivity

- Resistance to thermal shock

- Raw material is readily available at low cost without dramatic fluctuations

Different types of aluminum oxide can be found such as α, γ, η, Ɵ. The most stable form of alumina is α-alumina. Since this thesis is a chemical engineering thesis with an emphasis on catalysis and reaction, hence the applications of alumina in reactions are mentioned in the following paragraphs.

Pecchi et al. [59] used alumina as a support in a comparative study between Palladium-Cerium and Palladium-Lanthanum activities. The reported results showed the Cerium promoted catalyst on alumina had higher activity compared to Lanthanum promoted catalyst.

Alumina is a good choice to be used as catalyst support due to the reasons mentioned above but any improvement in this field would help this support to be more efficient. Researchers have found ways to improve alumina by making it a porous powder. Organized mesoporous alumina is a way to improve alumina efficiently. A very thorough review on synthesizing methods of organized mesoporous alumina was published by Marquez-Alvarez et al. [60]. These mesoporous alumina powders are mainly used in hydrodesulfurization, hydrodechlorination and some oxidation reactions. As an example for hydrodesulfurization application, Kaluza et al. [61] used organized mesoporous alumina with a surface area of 400-600 m2/g and pore diameter of 3-4.5 nm in desulfurization of thiophene. They could achieve a high loading on organized mesoporous alumina (30 wt%) compared to conventional alumina (15 wt%) and the activity was also reported to be two times higher so the 30 wt% loading was successful and there was no loss of activity in higher loading. Kim et al. [62] deposited Ni on mesoporous alumina in order to perform hydrodechlorination of 1, 2-dichloropropane.

Organized mesoporous alumina was also used to hydrogenate the cinnamaldehyde to cinnamyl alcohol by the deposition of Cu on alumina [63]. This type of alumina was used by Lenarda et al. [64] for the hydrogen production by methanol steam reforming with the help of Pd-Zn as active materials.

2.5. Lessons and challenges from literature review

From the literature review section, we can understand that understanding the catalyst behaviour is an important part of oil upgrading. Amongst the methods of oil upgrading, hydroprocesses give us an opportunity to have a flexible and efficient process, which can be modified to our favour by modifying the catalyst used in the process. Hydrodesulfurization is a way of improving the oil from an environmental point of view and it has recently gotten more attention due to restricted regulations.

Ring opening is one of desulfurization techniques, which can improve the fuel quality as well (cetane number improvement). In this study, ring opening of indan is the main reaction and iridium is used to perform this reaction as the active phase on structured and conventional supports since it was reported to have the highest activity for indan ring opening [28]. Structured supports are a result of the problems encountered when using a conventional fixed bed reactor. They have less pressure drop, are simpler to design and have better flow distribution.

Metal nano particles have a better activity and selectivity than conventional precursors due to their enormous surface area; hence they are a good candidate to be deposited on supports with limitations regarding the loading.

Alumina is counted amongst the best catalyst supports as a result of their high hardness, high compression strength, resistance to abrasion and chemical attack, high thermal conductivity and low cost.

Chapter 3. Experimental methods

3.1. Reactor setup

The reactor setup consists of one bubbler, one oven (Lindberg Blue M), one plug flow reactor (with a cover to block the flow of air from outside of the oven around the reactor while installed in the oven), 2 mass flow meters (Sierra Smart Trak 2), 2 tanks of Hydrogen and Argon, one gas chromatograph (GC) which is connected directly to the reactor outlet, 3 tanks of Hydrogen, Compressed air and Helium for the GC, heating tapes for tubes going into the reactor and a controlled temperature bath in which bubbler is located.

Fig.6. Schematic of the experimental setup
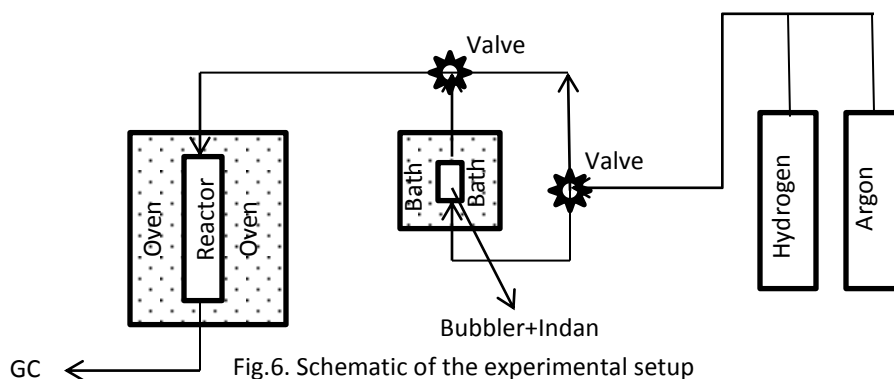
Hydrogen goes through the bubbler to get saturated from indan and then the reactants go to the reactor, which is installed inside an oven (the oven keeps the temperature of the reactor constant). After the reactor, the products go into the GC to get analysed. Before each test, the setup and reactor were purged using Argon followed by a reduction stage by Hydrogen, which helps to reduce any active metal particle that has not been reduced yet. The purging was done with

an Argon rate of 100 mL/min and the reduction was performed at 375°C for 1 hour with a Hydrogen rate of 80 mL/min.

The reactor (Fig.7) is tubular with a diameter of half inch and was packed in the following order:

- A piece of quartz wool at the end of the reactor

- ~17 grams of glass beads on the quartz wool

- Another piece of quartz wool on the glass beads

- 2 grams of silicon carbide (Mesh # 46)

- A mixture of catalyst and silicon carbide (Mesh # 150) or

- Round pieces of SMF on top of each other (for reactions with SMF),

- Another 2 grams of silicon carbide (Mesh # 46)

- Glass beads to the top of the reactor

The glass beads help to keep the catalyst in the center of the reactor (consequently the center of the oven) where the oven temperature is constant and is the same as the temperature which an internal thermocouple shows. Silicon carbide is for diluting the catalyst to prevent any hot spots in the reactor and mesh 150 has exactly the same particle size as the alumina powder used as catalyst support in this study (90 microns). Quartz wool is for filtering the

outcome gaseous products and to prevent the clogging of connection tubes and GC column.

The heating tapes can help to make sure that all of the reactants is going into the reactor in gaseous form and they are set at 220°C, which is above the indan boiling temperature (176°C).
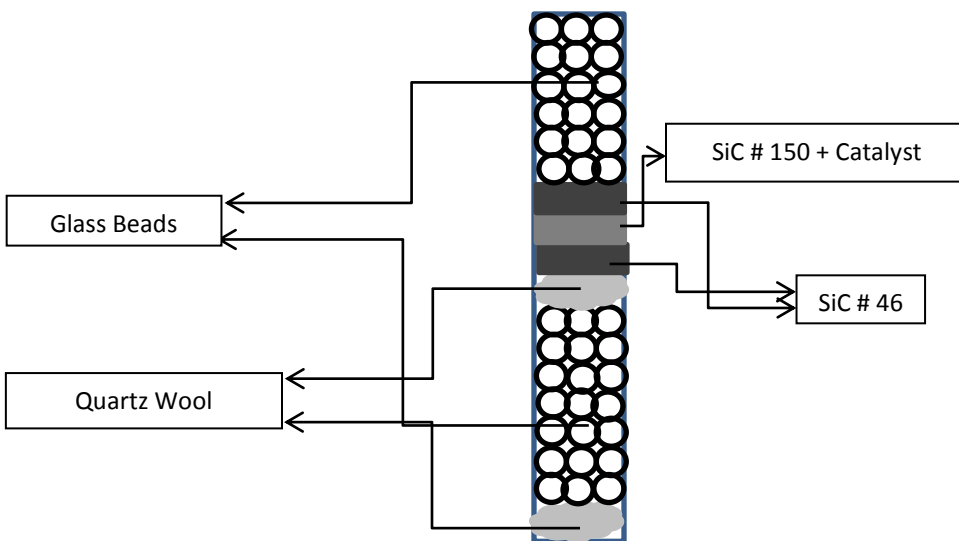

Fig.7. Schematic of the reactor

 The controlled temperature bath is for maintaining the temperature of indan constant to avoid any inconsistancy, which may occur if the indan temperature changes during a reaction or from day to day. All of the gas tanks were ordered from Praxair Canada.

Hydrogen, Helium and Argon were all ultra high purity (99.999%) and Air was extra dry (water ≤ 10 ppm). The GC which was used is a Varian 430 with a Flame Ionization Detector (FID). In order to clean the GC column each time after the tests, there were a shutdown run (during which the GC temperature goes higher than usual runs to desorb any contaminents remaining in the GC column) at the end of each day (without any components going into GC). After each test, the reactor was emptied and cleaned using tap water, acetone, versa (water+liquid soap) and milli-Q water.

3.2. List of materials

The following materials were used in this study: Indan (Sigma-Aldrich Canada, purity: 95%, boiling point: 176°C, melting point: -51°C, density: 0.965 g/mL at 25 °C), SMF (Bekipor ® ST DPF 701, N.V. Bekaert S.A., Zwevegem, Belgium, components: Al 3%, Cr 19-22%, C≤0.06, Mn≤0.04, Si≤0.06, P≤0.05, S≤0.03, Cu≤0.2, N≤0.03 and balance Fe, porosity: 80%, thickness: 0.3mm, weight: 450g/m^2), Ni nano particles (Sigma-Aldrich Canada, form: nano powder, particle size: ≤100mm, boiling point: 2732 °C, melting point: 1453 °C), Polyvinylpyrrolidone (Sigma-Aldrich Canada, average molecular weight: 40,000), Irridium (III) acetylacetonate (Sigma-Aldrich Canada, purity: 97%, form: solid, melting point: 269-271°C), Bis(cyclopentadienyl) nickel (Sigma-Aldrich Canada, form: solid, melting point: 171-173°C), Bis(acetylacetonato) Dioxomolybdenum (VI) (Sigma-Aldrich Canada, form: solid, melting point: 184°C), Toluene (Fisher

Scientific, boiling point: 111°C, melting Point: -95°C, density: 0.866 g/ml at 25°C),

Dichloromethane (Sigma-Aldrich Canada, purity: 99.8%, boiling point: 40°C,

melting point: -97°C, density: 1.325 g/ml at 25°C), Acetone (Fisher Scientific,

boiling point: 56°C, melting point: -95°C, density: 0.790 g/ml at 25°C), Methanol (

Fisher Scientific, boiling point: 64.7°C, melting point: -98°C, density: 0.791 g/ml

at 25°C), Iso-Propanol (Fisher Scientific, boiling point: 81-83°C, melting point: -

89.5°C, density: 0.785 g/ml at 25°C), hydrogen hexachloroiridate hydrate

(formula: $H_2IrCl_6 \cdot xH_2O$, Sigma-Aldrich Canada, purity: 99.98%, form: solid,

melting point: 65°C, density: 1.02 g/ml at 25°C).

Some representative molecular structures are shown below.
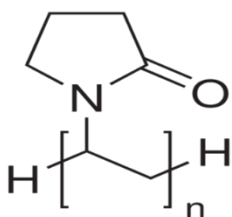
Polyvinylpyrrolidone
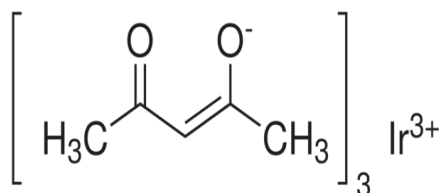
Iridium (III) acetylacetonate
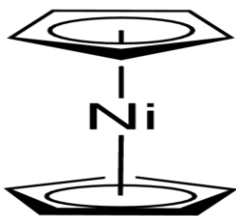
Bis(cyclopentadienyl) nickel
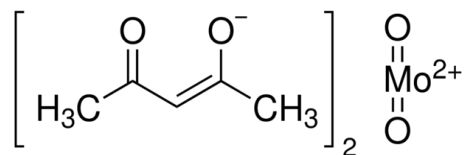
Bis(acetylacetonato) Dioxomolybdenum

3.3. SMF preparation

The SMF pieces were prepared by washing followed by a three stage heat treatment. The detailed procedure was as follows [2]:

- Circular SMF piece was cut and made sure that the circular SMF will fit in the reactor

- A hole was put on the SMF piece to make it easy for the SMF to stay on the hook, when it is placed into the furnace

- The SMF piece was cleaned with Toluene, Acetone, Methanol and Isopropanol prior to heat treatment

- The SMF piece was put in the furnace using a hook and a rod at 925°C for 55 minutes and then at 965°C for 1 hour and 5 minutes and then at 985°C for 2 hours

3.4. Catalyst characterization techniques

3.4.1. AAS

The concentration of nickel and molybdenum on SMF was measured using Atomic Absorption Spectroscopy (AAS) (Varian 220 FS unit using air and acetylene flame). The standard solutions were 0.5 ppm (by volume), 1.0 ppm, 3.0

ppm, 5.0 ppm and 10 ppm made by Shiraz Merali. The detection limit for Ni is 10 ng/mL and for Mo is 30 ng/mL.

3.4.2. SEM/AES

The Scanning Electron Microscopy (SEM) and Auger Electron Spectroscopy (AES) images were all taken and analysed by Shihong Xu with a JEOL Auger Microprobe JAMP 9500F. These images were used to investigate the deposition of iridium on SMF.

3.4.3. TGA

All of the TGA analyses were performed using a TA instruments TGA-Q500. The software package was TA Universal Analysis, which was used to illustrate the results of a TGA experiment. The sensitivity of TGA was 0.1 µg and for the mass loss, it was ±0.01%.

3.4.4. TEM

The TEM images were all taken with the help of Jing Shen by the TEM device located in Cross Cancer Institute (200kV JEOL JEM 2100). The samples for TEM images were prepared by grinding the impregnated α-Al_2O_3 to fine powder and then making a suspension of the powder in ethanol under ultrasonic treatment.

3.5. Ni & Mo deposition on SMF

The deposition of nickel was tested via incipient wetness impregnation method and all of the precursors were organic due to hydrophobicity of SMF pieces. Organic solutions typically wet ox-SMF surface and the amount is equal to 40% of the ox-SMF mass. In order to achieve 0.5% loading on ox-SMF, which weighed 0.043 grams a solution of 1.13 g-Ni/ 100g was needed. 0.113 grams of Ni nano-particles and 0.1 grams of PVP (as a stabilizer) were added to 9.82 grams of ethanol to make a precursor solution and the SMF piece was immersed in the precursor followed by a calcination at 200°C for 2 hours. A brief summary of the calculation is as follow:

0.4 X (SMF mass) = mass of the solution on SMF

0.005 (loading) X (SMF mass) = (the amount of active phase needed on SMF)

(The amount of active phase needed on SMF) X (the ratio of solid precursor mass to active phase mass) / (mass of the solution on SMF) = (the concentration needed for 0.5 wt.% loading)

Ni nanoparticles are not uniformly dispersed in ethanol, so the impregnation was performed in an ultrasonic bath to prevent the nanoparticles from

agglomerating. Ni loading was tested by placing the SMF piece in 10 mL of stirred nitric acid for 1 hour at 100°C to dissolve the Ni nano-particles in the nitric acid. The concentration of the outcome solution was measured via Atomic Absorption Spectroscopy to be 3 wt.%. Five pieces of SMF were prepared and tested in the reaction to see the activity of the catalyst on the support. The impregnation of SMF using organic Ni (bis-cyclopentadienyl-nickel in toluene) and Mo (bis-acetylacetonato-dioxomolybdenum VI in DCM) precursors was exactly the same as Ni nano particles except it was not done using an ultrasonic bath.

3.6. Ir deposition on SMF

In this study, the deposition of iridium was tested through incipient wetness impregnation and drop method impregnation. The catalysts prepared via incipient wetness impregnation method showed no activity in the ring opening reaction therefore the either the target active metal loading had not been achieved or the active metal particles on SMF had agglomerated. All of the precursors were made of organic solvents or a mixture of water and organic solutions due to the hydrophobicity of the SMF.

Incipient wetness impregnation method is a method to impregnate conventional catalyst supports such as powders with the precursor solution of the volume just enough to fill the support pores. In the case of SMF with low surface area and panel 3-D structure, the low allowed liquid precursor volume and its in-depth

penetration may result in having lower amount of active metal particles in a non-uniform condition. This method procedure was done as follows.

3.6.1. Precursor and impregnation

The first precursor was made of iridium (III) acetylacetonate in toluene. The concentration of the precursor solution was determined by calculating the amount of toluene absorbed by SMF and knowing the targeted loading on the SMF. One SMF piece can absorb an amount of toluene equal to 40% of its mass (based on measurements done in the laboratory). For 1% loading, a precursor solution with the concentration of 0.062 mg/mg-solution was needed. The SMF pieces were immersed into this precursor and then dried under laboratory air followed by a calcination step, which was performed at 350°C for 3 hours. The samples prepared by calcination at 350°C for 3 hours were named C-1. The next samples, C-2 and C-3, were prepared just the same way as mentioned above except the calcination steps, which were performed at 300°C and 320°C for 3 hours respectively.

The next precursor used in this study was made of Hydrogen hexachloroiridate (IV) hydrate in a mixture of water and ethanol. The method is called "Alcohol Reduction" and has been used on conventional catalysts (powder alumina). The desired amount of iridium solid precursor was calculated the same way as mentioned above. The solid iridium precursor was dissolved in 50ml of water

and the solution was transferred to a 3-neck flask. A solution of ethanol and water (47ml and 70ml respectively) was added to the flask followed by adding 0.222g amount of PVP as stabilizer. A magnet stir bar was put on the bottom of the flask to provide a good stirring and the flask was connected to a condenser to prevent losing of precursor during boiling. The flask was heated with the help of a heater, which was put under the flask and then the solution was kept in boiling temperature for 3 hours. During these 3 hours the solution changed color many times due to different complexes of iridium, which were formed as a result of reduction of iridium. The final precursor was known to have iridium nano-particles (verified by TEM images) and was ready to be used as catalyst [73]. For the first attempt, 0.06 grams of solid precursor was used and the final solution was dried in a rota-vap and then 1.6ml of ethanol was added to the dried solution in order to meet one-immersion concentration. Table.2 summarizes all of the samples used in this thesis.

Table.2. Samples calcination and precursor conditions

Sample name	Ir active phase source	Calcination steps	Used support
C-1	Iridium III acetylacetonate in toluene	350°C for 3 hours	SMF
C-2	"	300°C for 3 hours	"
C-3	"	320°C for 3 hours	"
M-1 (loading= 0.06 wt.%)	PVP stabilized preformed nanoparticles	300°C for 1 hour	γ-Al$_2$O$_3$ powder
M-2 (loading= 0.13 wt.%)	"	"	"
Drop method	"	"	SMF

samples (loading= 0.125 wt.%)			
Temperature effect samples (loading = 0.22 wt.%)	"	"	γ-Al_2O_3 powder
A-1 (0.22 wt.% Ir, 3.5 wt.% PVP)	"	No calcination	"
A-2 (0.22 wt.% Ir, 3.5 wt.% PVP)	"	300°C for 1 hour	"
A-3 (0.22 wt.% Ir, 3.5 wt.% PVP)	"	300°C for 1 hour and reduction under hydrogen at 375°C for 1 hour	"

3.6.2. Drop method

The precursor solution for this method was prepared the same way as mentioned above (Ir nanoparticles via alcohol reduction) but the impregnation method was to put drops on the SMF and let it dry overnight (after each drop). The amount of drops was calculated knowing the target loading and the concentration of the precursor solution. In this study to achieve 0.4% loading, 2 drops were needed.

3.7. Temperature effects on RO reaction using powdered catalyst

In this section, the effect of temperature has been investigated to see how the conversion and selectivity would change by setting the temperature at 350°C, 360°C and 370°C. Reactor packing and conditions were all the same as indicated in the experimental section (Hydrogen flow at 50 mL/min) and 0.4 grams of catalyst with a loading of 0.22 wt % (T-1) was used and diluted in 1.6 grams of silicon carbide.

3.8. Powdered catalyst activation energy

In this section of the studies, we focused on finding activation energy for indan ring opening using powdered γ-Al_2O_3 as support and iridium as active metal. The batch used in this experiment had a loading of 0.23 wt% and in each reaction test, 0.27 g of the catalyst was used and diluted with 4.73 g of silicon carbide. The activation energy studies were performed based on 4 temperatures, which are 350°C, 360°C, 370°C and 380°C. The tests were carried out twice at each temperature to check the reproducibility.

3.9. Madon-Boudart test

This test has been explained in the literature review chapter (subchapter 2.1.4). Two batches of M-1 and M-2 having 0.06 wt% and 0.13wt% iridium loadings respectively were prepared using alumina powder ($ɣ$-Al_2O_3 porous powder) and the impregnation was done using incipient wetness method. The tests were performed under different conditions to investigate the flow rate and silicon carbide needed in order to have no mass and heat transfer limitations. The experiments were all done at 350°C and 380°C (since all of the experiments were carried out between these two temperatures). In these tests, it is very important to have the same amount of active phase at each temperature and flow rate. The experiments were done under the following conditions:

Table.3. Madon-Boudart tests conditions

	First set		Second set		Third set		Fourth set	
Catalyst mass (g)	1 M-1	0.5 M-2	0.7 M-1	0.35 M-2	1.2 M-1	0.6 M-2	0.8 M-1	0.4 M-2
Al_2O_3 (g)	0	0.5	0.3	0.65	0	0.6	0	0.4
SiC # 150	3 g	3 g	3	3	3	3	4.2	4.2
H_2 flow (mL/min)	80	80	80	80	120	120	120	120
Temperature (°C)	350	350	380	380	350	350	380	380

3.10. Investigation of PVP removal using thermo gravimetric analysis

The catalyst used in this section was prepared via alcohol reduction method and the loading was 0.22 wt % Ir on ɣ-Al$_2$O$_3$ using 3.5 wt % PVP as stabilizer. The dried powder after deposition of active metals via incipient wetness impregnation was used as sample A-1 (not calcined). The A-2 was the catalyst, which was calcined at 300°C for 1 hour. The A-3 sample was the A-2 sample after reduction in the reactor at 375°C and a hydrogen rate of 80ml/min for 1 hour. All of the samples were heated from 25°C to 800°C at the rate of 5°C/min under nitrogen atmosphere.

Chapter 4. Results and discussion

4.1. Ni & Mo deposition on SMF

As was shown by Cheng et al. [72] Ni catalyst with a powdered γ-Al$_2$O$_3$ as a support showed hydrogenation activity in the hydrotreatment of indan, but no conversion could be achieved when corundum was used as a support, or when SMF was impregnated with an organic Ni precursor, most likely due to the large Ni particle size. In the current study, we attempted to use commercial Ni nanoparticles (<100nm) for the deposition. The use of Ni nanoparticles allowed 3 wt.% deposition on SMF pieces as verified by AAS. The structured material was subjected to ultrasonic adherence test to verify the mechanical stability of the deposited Ni nanoparticles, and the SEM images taken before and after the ultrasonic treatment showed excellent stability of the material (Figs. 8 and 9). However, when 5 pieces of 3 wt.% loaded SMF (each piece was weighted around 0.04 g) were tested in the hydrotreatment of indan, no catalytic activity was found (H$_2$ flow of 50 mL/min at 350°C).

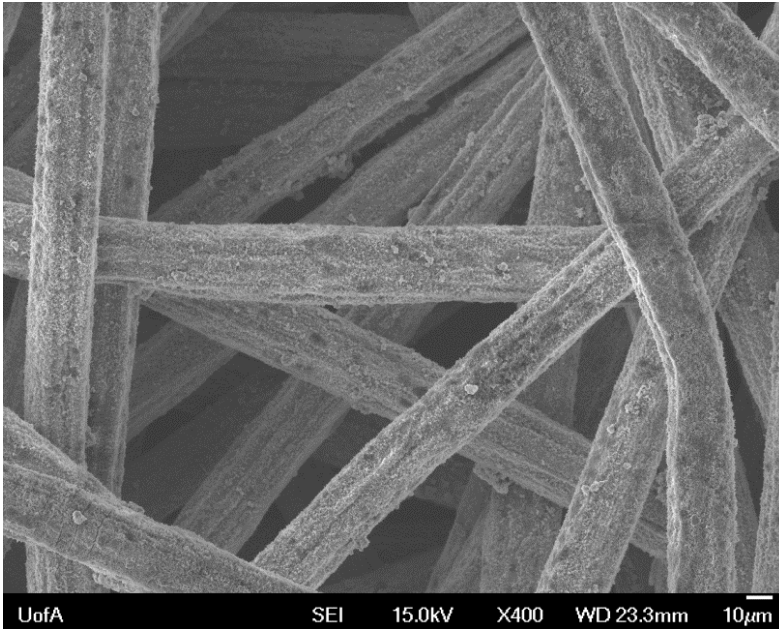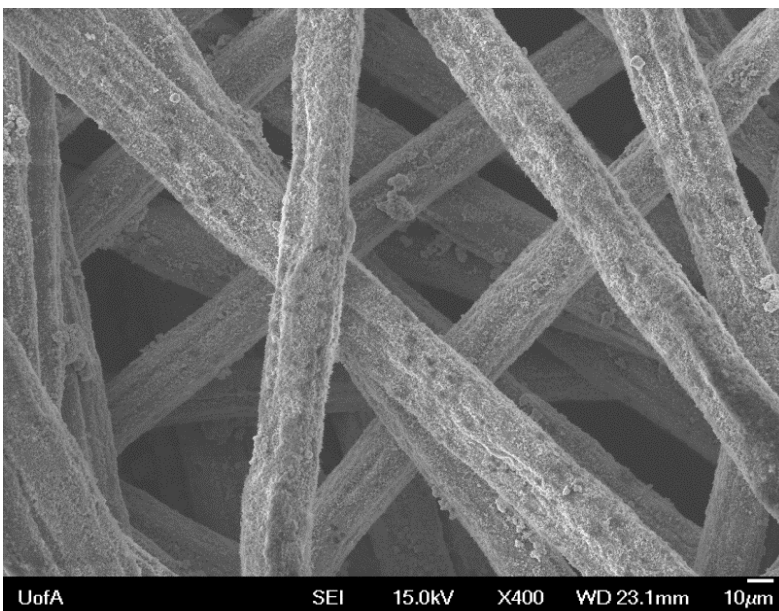Fig8. SEM picture of SMF with deposited Ni nanoparticles - before ultrasonic treatment

Fig.9. SEM picture of SMF with deposited Ni nanoparticles – after ultrasonic treatment

The 4-fold increase of Ni nanoparticle loading did not result in the conversion increase. To improve the catalyst activity, Mo was added as a second metal as Ni-Mo catalysts are commercially used in hydrotreatment [15]. The targeted

loadings were 3 wt.% for Ni and 12 wt.% for Mo using oleophilic bis(cyclopentadienyl) nickel dissolved in toluene and bis(acetylacetonato) dioxomolybdenum (VI) dissolved in DCM. These precursors were selected due to the hydrophobicity of the oxidized SMF to ensure its wetting with the metal precursors. After the impregnation, the material was calcined first at at 140°C for 1 hour for remove solvents followed by 450°C calcination for 2 hours to decompose organic precursors. When the NiMo active phase was deposited on powdered corundum, the catalyst allowed 12% conversion in indan ring opening (0.7 g of the catalyst). Unfortunately, such metal loadings were too high to remain intact when deposited on SMF and could be easily removed with the touch of a finger. The use of polymer PVP as a binder which is typically used to adhere powders to arranged substrates did not improve the stability. Lower loadings would lead to no catalytic activity since 3 wt.% Ni and 12 wt.% Mo (which is rather high loading) showed us a relatively low conversion of 12%.

According to the obtained results, Ni and Mo are not suitable active phases to be deposited on SMF for the hydrotreatment reactions due to their low activity and the restrictions regarding SMF loading. Hence, a more active phase should be selected to allow high activity at low metal loadings on the catalyst and practical catalyst loadings in the reactor.

4.2. Nano-Ir/SMF and its activity in indan RO

Ir is known to be the most active metal in indan RO [29], so it was selected as an active phase for the deposition on SMF. Some of the precursors (such as iridium (III) acetylacetonate) have been investigated but there was no activity observed and the probable cause can be the calcination step. At some temperatures (300-350°C) the iridium precursor evaporated so there was no iridium left on the support.

To ensure the catalyst activity, the iridium active phase was preformed as PVP-stabilized Ir nanoparticles and then deposited on the oxidized SMF. The formation of Ir nanoparticles of ~ 2nm size was performed according to a known technique developed by J. Shen [73]. The Ir loading as determined by Neutron Activation Analysis (NAA) was 0.125 wt.%. SEM and AES of the final Ir/SMF material were used to investigate if there was iridium on the surface of SMF or not and to check how far the nanoparticles can penetrate into the metal fibers mesh from their colloidal dispersion in ethanol. From Fig. 10 one can see the surface of a treated SMF (with whiskers) and the sample points for AES test (which can show us the local elemental analysis of the surface). All of the points showed identical composition (Fig. 11). The interpretation of the AES graph was done based on the characteristic Auger peaks for Ir and Al. Fig. 12 shows the cross section of the Ir/SMF material and sample points for AES analysis. Only

points 1-4 gave reliable information due to the device restrictions. The device restrictions occur when a sample point has some obstructions which would make it impossible for the electron to come back to the detector leading to a result without any elements. The AES data for points 1 and 2 showed the presence of iridium but for points 3 and 4 the data did not show much trace of iridium suggesting that only external SMF panel surface is loaded with the active metal.
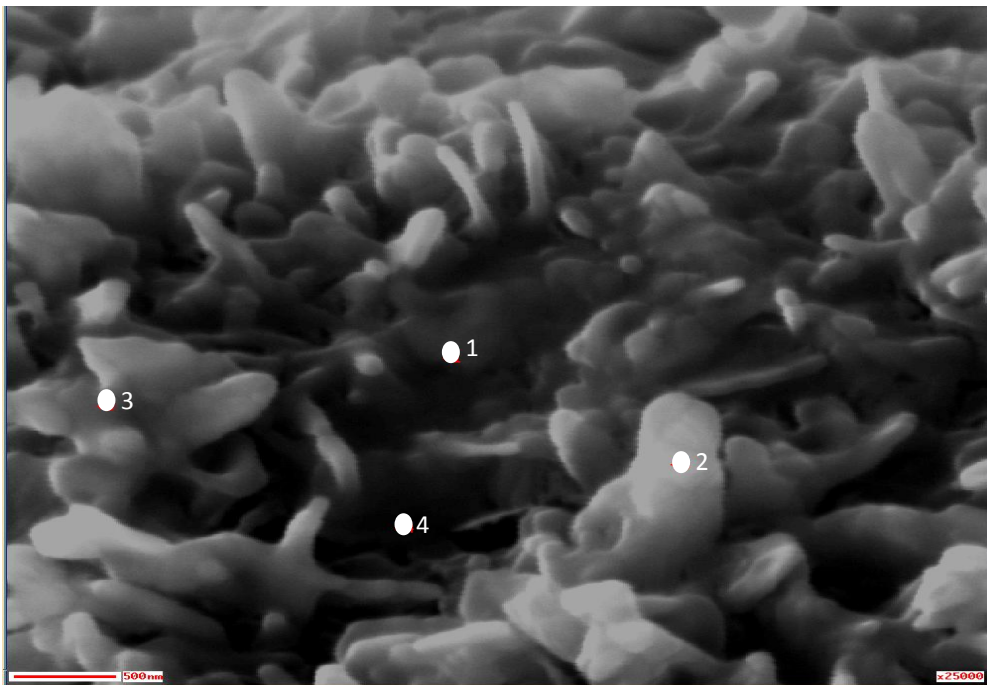

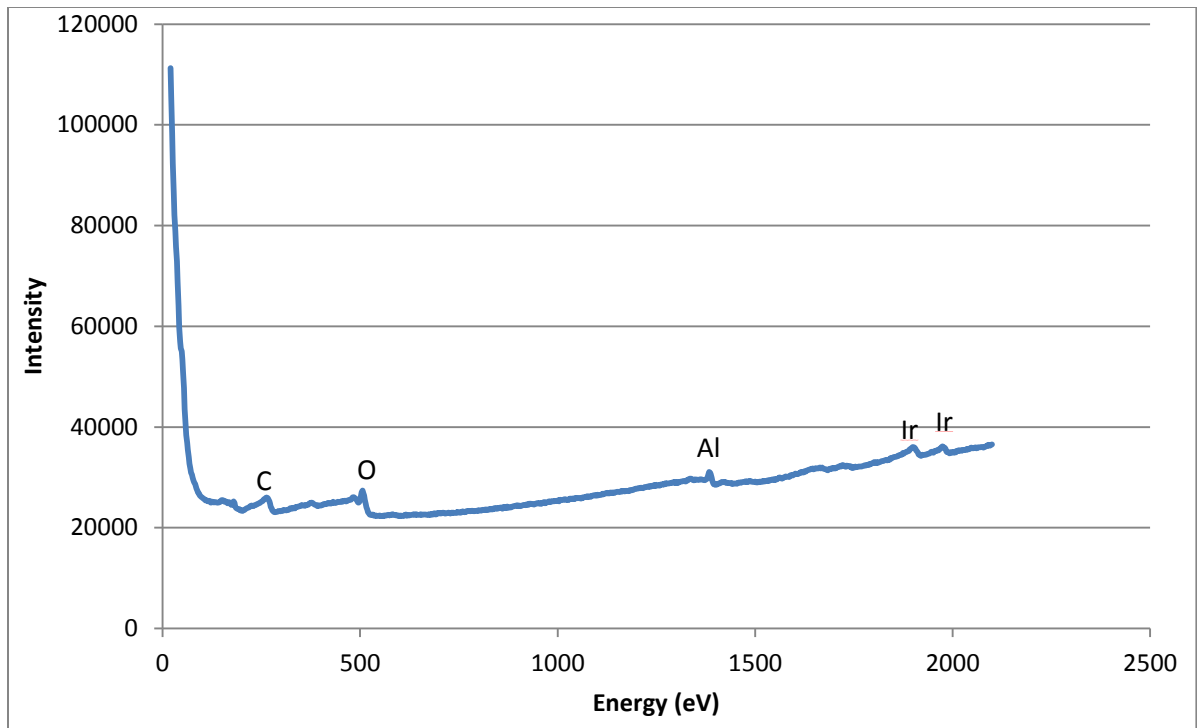Fig. 10. SEM image of nano-Ir/SMF material with points used for AES analysis

Fig. 11. AE spectra for all points 1-4 from Fig. 10 are shown but are seen to completely overlap
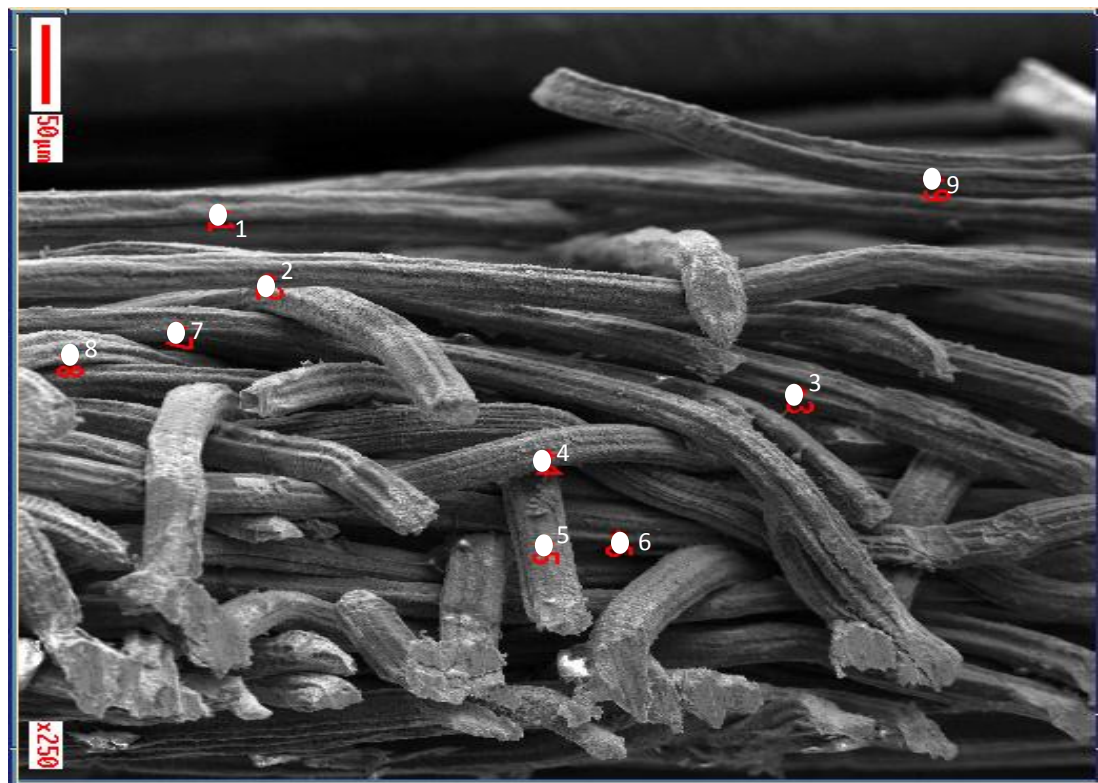
Fig.12. SEM picture of SMF cross section after iridium deposition, the points are the AES sample points
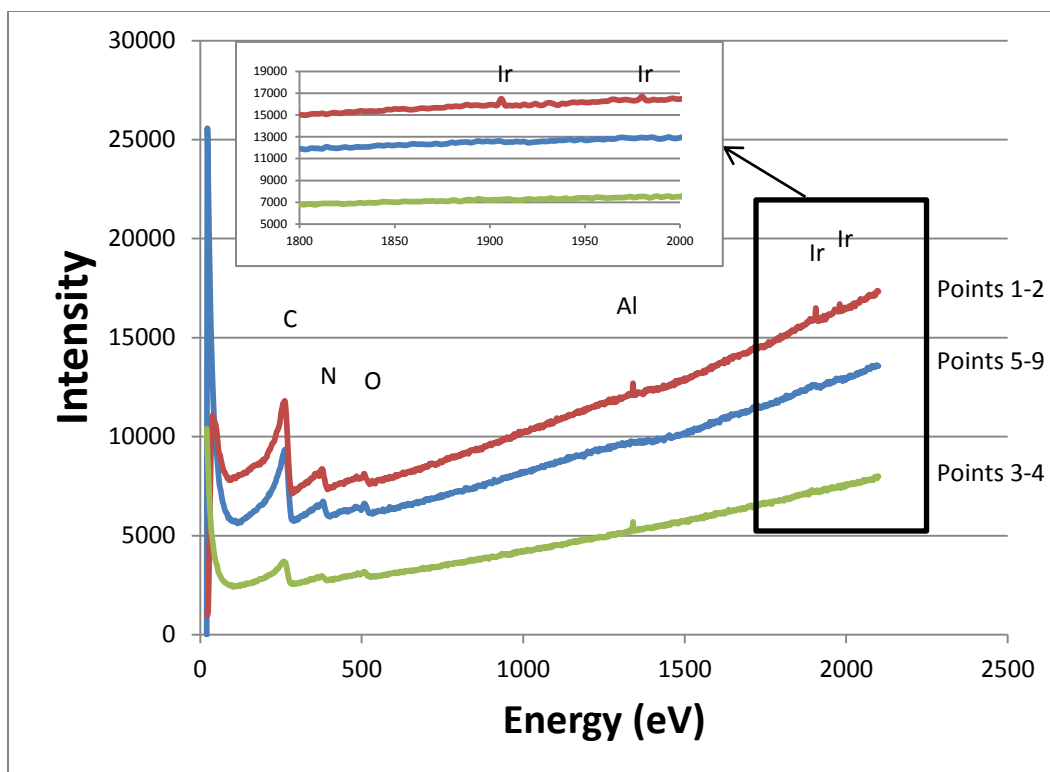
Fig.13. AE spectra for points 1-9 from Fig.12

With the Ir nanoparticles located on the external surface area of the SMF panel, no internal mass transfer limitations (MTL) may be anticipated in the RO reaction. To verify the absence of the external MTL, three tests were performed. In the first test, the amount of catalyst was 0.22 g and the flow rate was 25 mL/min; for the second test, these parameters were doubled and for the third were increased four times. The indan conversions at 350°C were 5.0%, 4.2% and 5.8% respectively indicating the absence of external MTL for the nano-Ir/SMF catalyst.

The differential reactor conditions allowed us to estimate the reaction activation energy.

Rate=K· [Indan]$^{\alpha}$· [Hydrogen]$^{\beta}$ (Eq.5)

Rate=ΔC/t (Eq.6)

X=ΔC/C$_0$ (Eq.7)

K=A.e^(-E$_a$/R$_g$·T) (Eq.8)

From eq.5 to eq.8 :   X·C$_0$/t· [Indan]$^{\alpha}$· [Hydrogen]$^{\beta}$·A=e^(-E$_a$/R$_g$·T) (Eq.9)

C$_0$, t, [Indan], [Hydrogen], A, E$_a$ and R$_g$ = Constant (Eq.10)

C$_0$/t· [Indan]$^{\alpha}$· [Hydrogen]$^{\beta}$·A = C1 (Eq.11)

X·C1 = exp (-E$_a$/R$_g$·T) (Eq.12)

Ln(X)= -E$_a$/R$_g$.T – Ln(C1) (Eq.13)

Fig.14 displays the Arrhenius plot. 10 pieces of SMF were impregnated and tested in reaction each time and this was done for temperatures 360°C to 380°C and 5 times at each temperature. The average conversions of the 5 runs for 360°C, 370°C and 380°C were observed to be 4.18%, 4.85% and 5.08% respectively. Due to the low conversions, we can assume that the concentrations of reactants were almost constant during reaction and knowing that the retention time for the reactants was constant (same reactor volume and same reactants` flow rate each time), we can conclude that if we draw Ln (X) vs. 1/T (X

57

is conversion), the data points should be on a line and the slope of that line is -E_a/R (E_a is activation energy and R is universal gas constant). 5 GC runs for each temperature were performed; the graph shows the average data for conversion with error bars (the error bars are + one standard deviation). The activation energy using Eq.13 was found to be 34±4 kJ/mol.
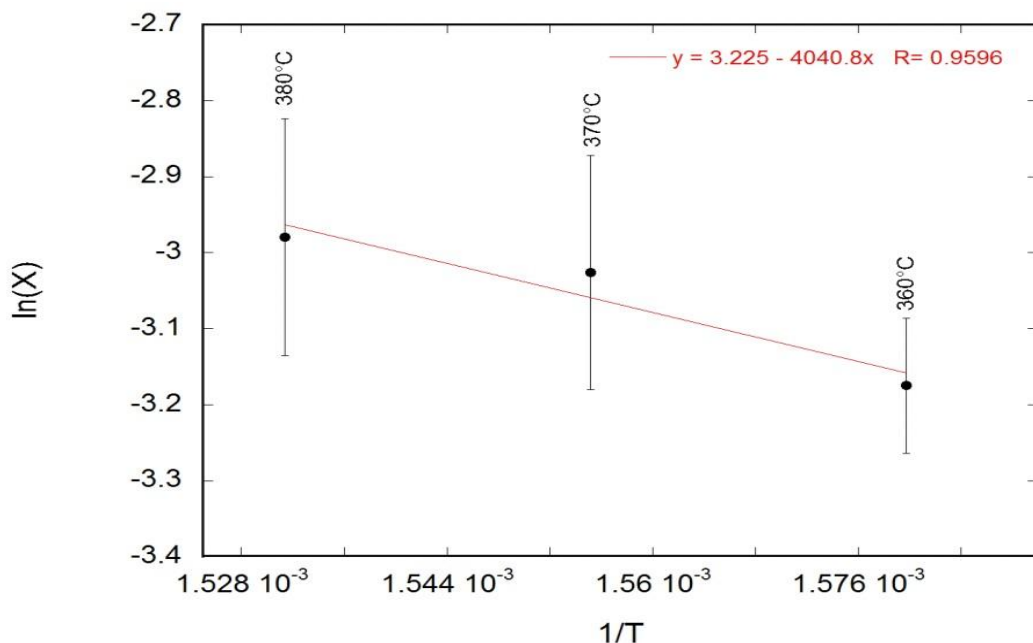
Fig.14. Arrhenius plot for the indan RO at differential conditions : 0.44 g catalyst with 0.125 wt% loading and hydrogen flowrate of 50 mL/min

To verify if the FeCrAl alloy material impacts the Ir catalytic behavior, Ir nanoparticles were also deposited on powdered corundum (as mainly α−alumina is formed upon FeCrAl alloy thermal oxidation). The Ir/corundum catalyst allows 7.1% indan conversion per milligram of Ir vs. 7.6% conversion for the Ir/ox-SMF material indicating that the catalytic properties are not affected by the bulk support material in terms of Ir activity.

As seen from the above data, the Ir/SMF material is active in the ring opening of indan and the use of the structured support allows eliminating the MTL, thus, it can be regarded as a promising alternative to powdered catalysts.

4.3. Nanostructured iridium on powdered ɣ-Al$_2$O$_3$ support

In order to achieve practically high conversions in indan RO, Ir loadings on a catalyst support must be increased, which can be easily achieved by using a support with higher surface area, such as ɣ- Al$_2$O$_3$. The preformed Ir nanoparticles deposited on the powdered gamma-alumina was used for further studies.

4.3.1. Verification of absence of mass and heat transfer limitations

The well-known Madon-Boudart test was used to verify the absence of mass and heat transfer limitations in indan RO reaction. The details of calculations for this test have been discussed in section 2.1.4. At a hydrogen flow rate of 80 mL/min at 350°C, the first set of conversions were 35% and 42% for 1 g of M-1 sample of Ir/ɣ-Al$_2$O$_3$ catalyst (Ir loading of 0.06 wt .%) and 0.5 g of M-2 sample (Ir loading of 0.13 wt %), respectively. Fig. 15 shows Ln (conversion per grams of catalyst used) versus Ln (loading of catalyst). Each point shows the average of two experiments.

Fig.15. Madon-Boudart test for the indan RO reaction at 80 mL/min H_2 flow rate at 350°C and 380°C (two points were obtained for each temperature and they may not be clearly seen due to the close proximity)

From Fig. 15, the slope of the line is 1.13, which is close to unity; therefore we can say that there is a negligible effect of mass and heat transfer limitations under these conditions. However, at 380°C, 0.7 g of M-1 and 0.35 g of M-2 with H_2 flow rate of 80 mL/min the slope becomes 0.3. As the slope is far from unity, the mass and/or heat transfer limitations exist at this higher temperature and the results cannot be considered for kinetic regime activation energy calculations.
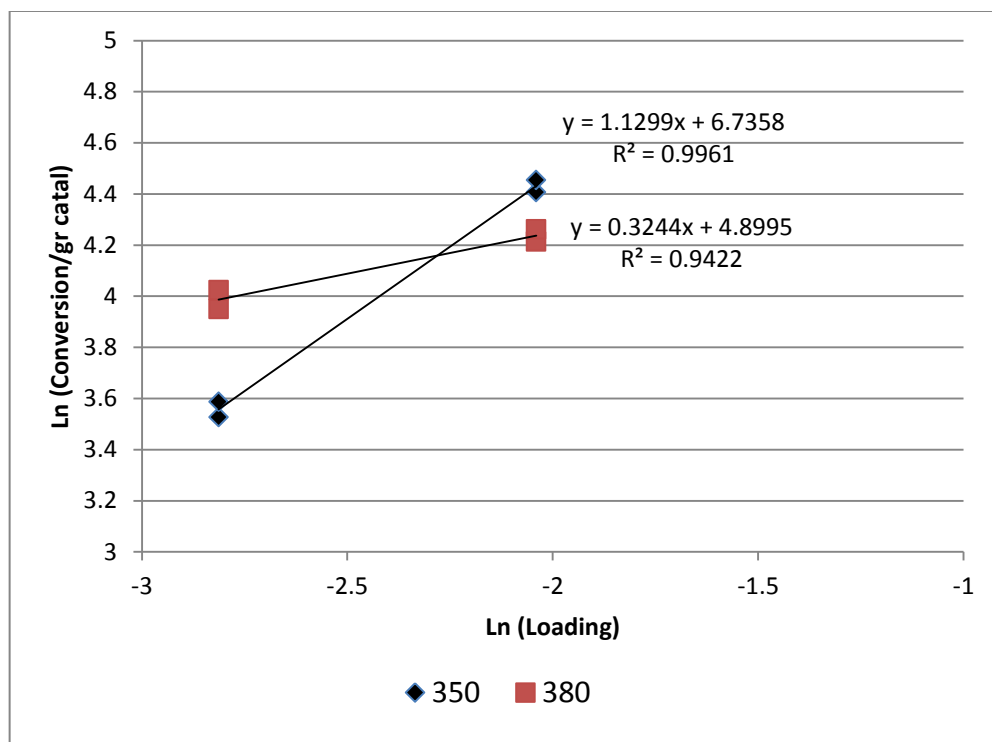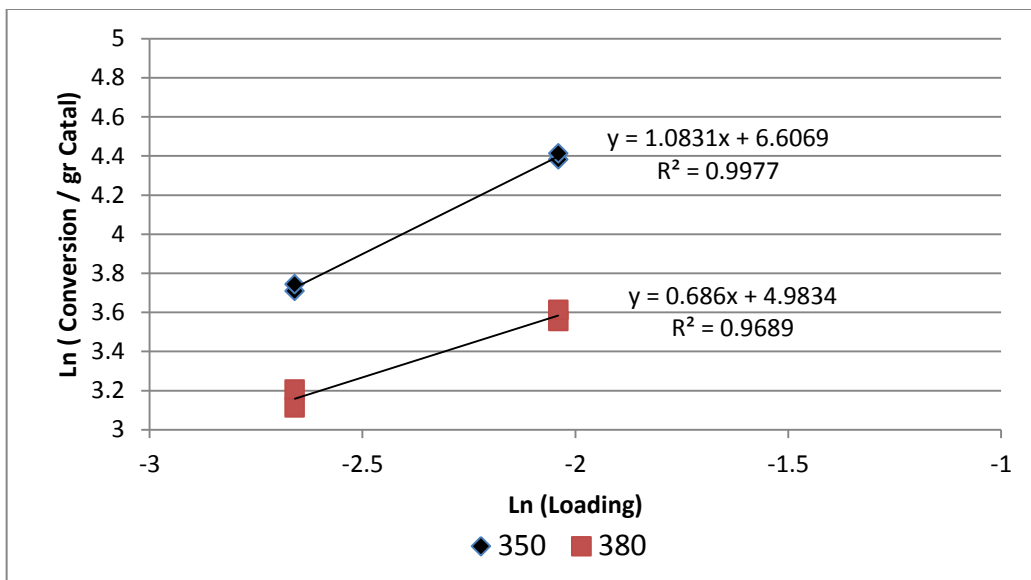
Fig.16. Madon-Boudart test for the indan RO reaction at 120 mL/min H_2 flow rate at 350°C and 380°C (two points were obtained for each temperature and they may not be clearly seen due to the close proximity)

In order to overcome possible mass transfer limitations, in the subsequent experiments the H_2 flow rate was increased to 120 mL/min. At 350°C, the conversions were 50% and 49% (average of two experiments) for 1.2 g of M-1 and 0.6 g of M-2 catalyst samples, respectively. The slope of Madon-Boudart graph was 1.08 which indicates the absence of mass and heat transfer limitations (Theoretically the slope cannot be more than one but in experimental cases due to measurement errors occurring by both the device and researcher, it was found to be a little greater than one). The Madon-Boudart graph slope at 380°C was 0.7 for 0.8 g of M-1 and 0.4 g of M-2 (with average conversions of 19% and 14%, respectively) which is relatively close to unity and the absence of transport limitations may be assumed.

The absence of internal mass transfer limitations was also confirmed by estimating the Weisz-Prater number. The observed reaction rate was used to determine the absence of internal mass transfer limitations. C_{WP} (the Weisz-Prater parameter) is defined as eq. 13 [65]:

$$C_{WP} = \eta \times \phi_1^2 \qquad \text{Eq.13}$$

where η is the ratio of the observed reaction rate to the reaction rate evaluated at the surface concentration of reactant C_{As}, and ϕ_1^2 is the ratio of the reaction rate evaluated at the surface concentration of reactant C_{As} to diffusion rate. The criterion is quantitatively defined as [65]:

$$C_{wp} = -r_A(\text{observed}) \, \rho_c R^2 / (D_e C_{As}) \qquad \text{Eq.14}$$

where $-r_A$(observed) is the observed rate of reaction (mol indan/grams of catalyst.second), ρ_c is the catalyst density which is assumed the same as alumina density (3.67 g/ml, since the loading on alumina is very low), R is the radius of alumina particles (0.005 cm), C_{As} is the surface concentration of indan (mol/ml) which is the same as the bulk concentration (since the absence of external mass transfer limitations was verified by Madon-Boudart test) and D_e is the effective diffusivity defined as [68]:

$D_e = D\varepsilon\delta/\tau$

where D is diffusivity coefficient (m^2/s), ε is porosity, δ is constrictivity and τ is tortuosity and the amounts of these parameters are 0.2925, 0.4, 0.8 and 2 respectively [68]. If C_{wp} is far less than unity, then there is no internal mass transfer limitation but if C_{wp} is much higher than unity, then there is a severe case of internal mass transfer limitation. As an example, a conversion of 50% was used for calculations (the conversion of M-1 sample from the third set of Madon-Boudart tests) where the hydrogen flow rate was 120 mL/min and indan concentration was 940 ppm. Knowing the silicon carbide and alumina density (1.44 g/ml, 3.67 g/ml) and the amounts used in the reaction (3 g SiC, 1.2 g alumina), we can calculate the reactor bed volume (2.38 mL). Hydrogen flow rate of 120 mL/min (2 mL/s) means a retention time of 1.19s; the actual rate of the reaction can be calculated as the conversion times the reactor volume and indan concentration divided by retention time and mass of the catalyst. The Weisz-Prater parameter can be calculated to be 0.00007 which is much smaller than unity. This indicates the absence of internal mass transfer limitations.

Table.4. Weisz-Prater calculations

-r$_A$(observed)/C$_{As}$	p_c	R	D$_e$	C$_{wp}$
362 [ml/gr.s]	3.67 [g/ml]	0.00005 [m]	0.0464	0.00007

Thus, at hydrogen flow rate of 120 mL/min no mass or heat transfer limitations were observed, and at these conditions the activation energy studies may be performed in the kinetic regime.

4.3.2. Influence of temperature on the indan RO selectivity

Temperature is known to influence the selectivity in ring opening and hydrogenation reactions. For example, Boutonnet et al. [29] reported that at 40 bar and 320°C using 2 wt.% $Pt_{25}Ir_{75}$/boehmite, the hydrogenation of indan to hexahydroindan had its highest yield and for the ring opening, 400°C was mentioned as the highest yield. It was also reported that at temperatures above 320°C the selectivity changes from hexahydroindan to dehydrogenation or cracking products such as indene, n-propylcyclohexane and ethylcyclohexane. This part of the thesis was done to gain more understanding of the temperature influence on indan RO reaction using presynthesized Ir nanoparticles as well as activation energy studies. The reactions were done under 50 mL/min flow of hydrogen using 0.4 g of catalyst T-1 with a loading of 0.22 wt % (using preformed Ir nanoparticles as active phase). Fig. 17 shows the conversion trend at different temperatures and times. The selectivity is calculated as the ratio of the concentration of a specific product to the concentration of all of the products. The conversion is calculated as the ratio of indan concentration difference (before and after reaction) to indan initial concentration (before reaction). The yield is the mathematical product of selectivity and conversion.
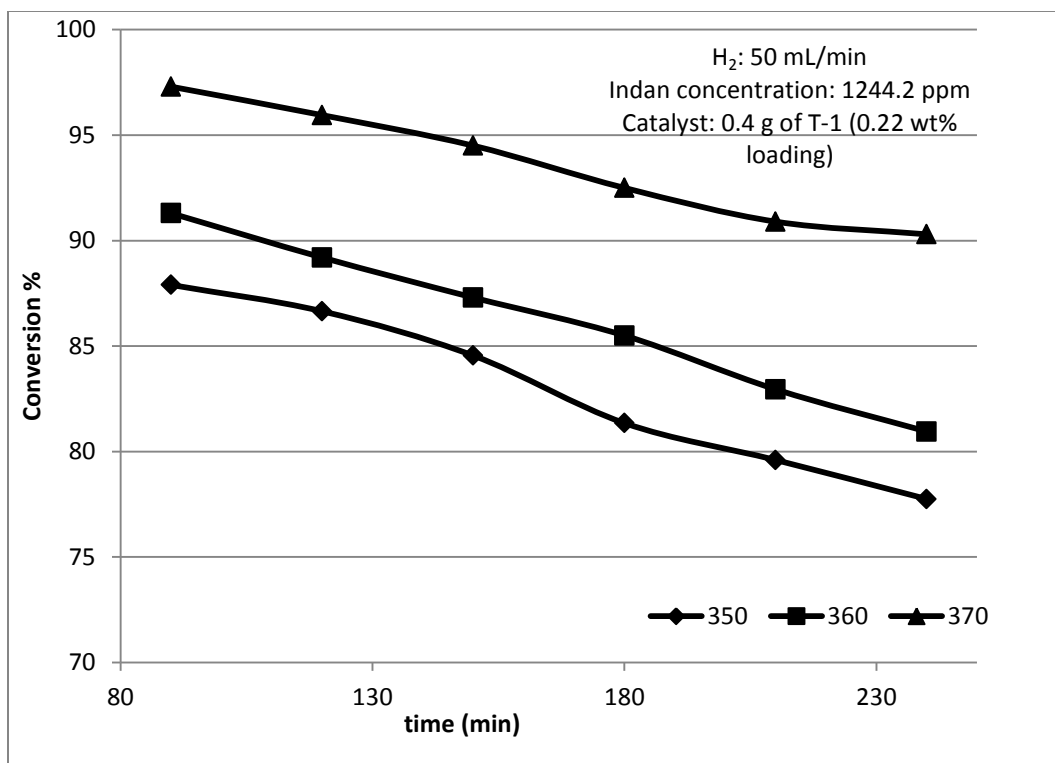
Fig.17. Indan ring opening conversion at different temperatures (°C) versus Time on Stream (min)
The lines between data points are to guide eyes only

From Fig. 18 we can calculate the catalyst decay d(t) at different temperatures.

The catalyst decay is defined as the ratio of conversion at time t to the initial

conversion [65].
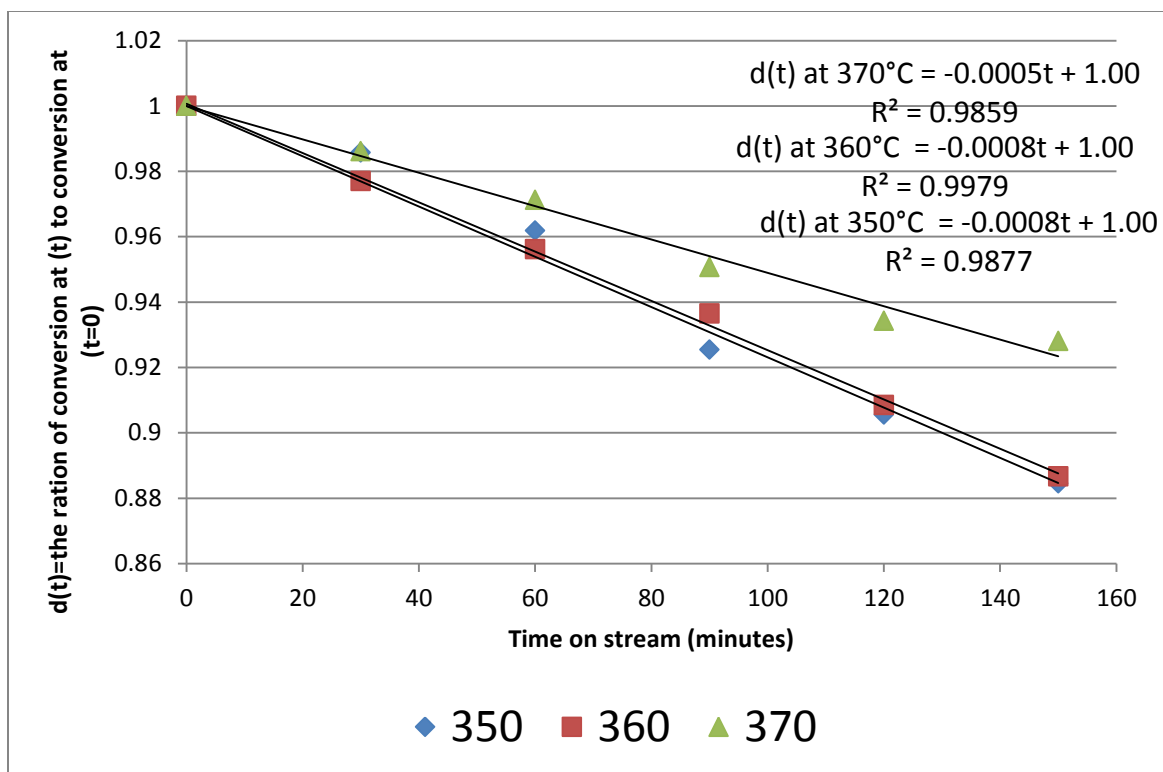
Fig.18. Catalyst activity at different temperatures (°C) versus Time on Stream (min)

As we did not perform the kinetic modeling, the deactivation is only showed by the decrease in indan conversion (using the t=0 conversion as reference) per minute. The reduction rate of indan conversion was the same for 350°C and 360°C (0.0008) while this rate was 0.0005 for catalyst operating at 370°C.

The deactivation in this reaction most likely occurred due to coke deposition which was also reported by Nylen et al. [29]. The carbonaceous deposits block active sites or cover the surface of catalyst and prevent them from being available and performing their role in the reaction. The amount of coke deposited on active sites was found to be 1.5 wt% [29]. The coke components depend on how they formed (in this case: indan ring opening), the age of the

catalyst, the type of catalyst (in this case: Ir nanoparticles) and the conditions of the reaction (temperature and pressure). It has been reported that coke formation for the reactions with hydrogen acceptor feeds such as olefins (in this case: indan) occurs faster [74, 75]. Sintering is another possible deactivation reason which usually occurs for metal catalysts both supported and unsupported. Sintering is mostly affected by temperature and less affected by atmosphere condition [76].
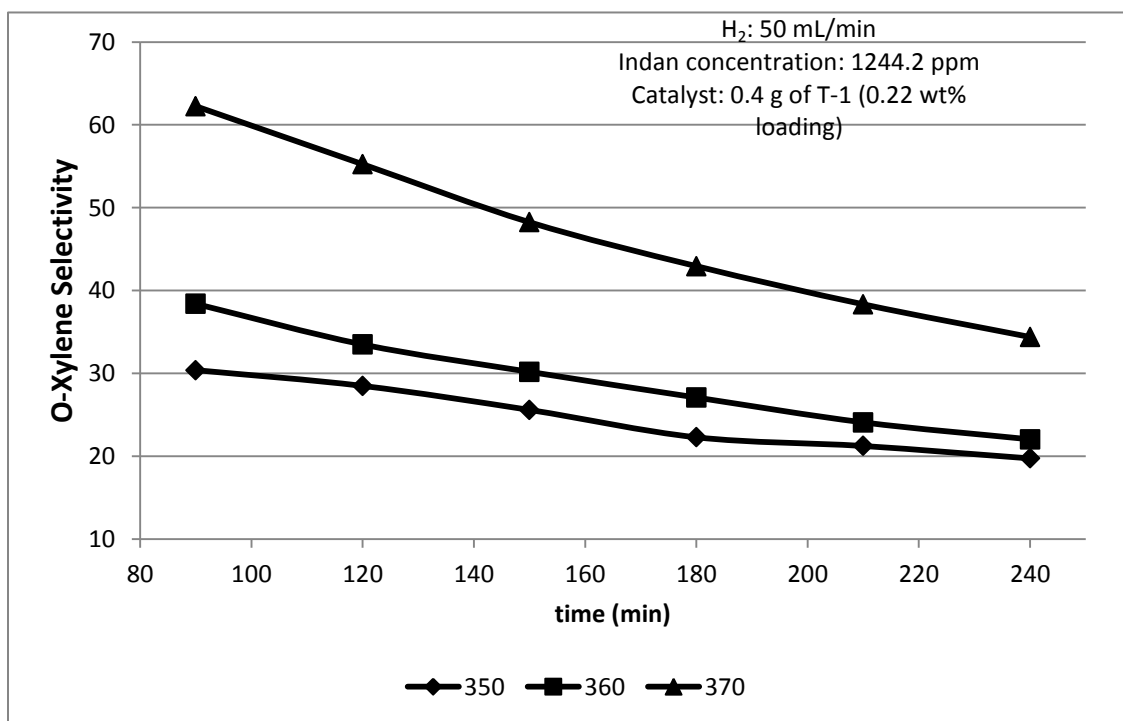

Fig.19. O-Xylene selectivity at different temperatures versus Time on Stream (min)
The lines between data points are to guide eyes only
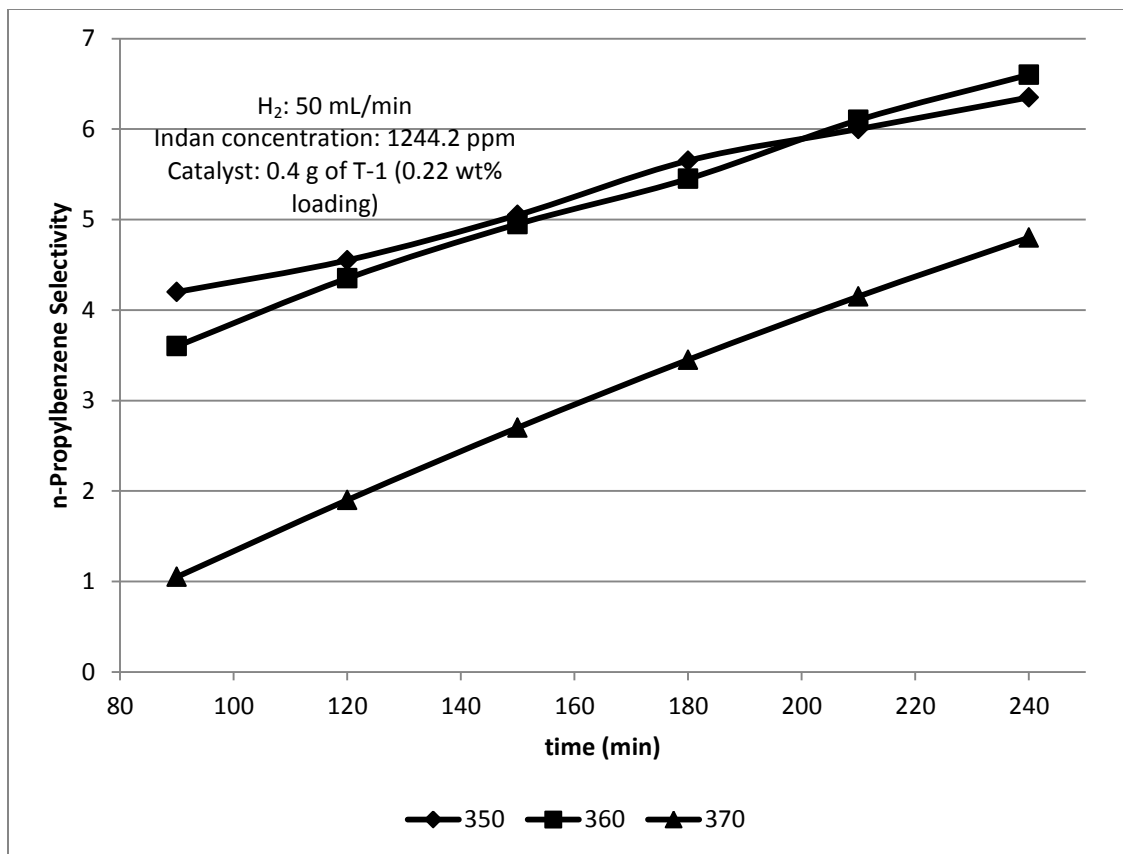
Fig.20. n-Propylbenzene selectivity at different temperatures versus Time on Stream (min)
The lines between data points are to guide eyes only

Fig.21. 2-Ethyltoluene selectivity at different temperatures versus Time on Stream (min)
The lines between data points are to guide eyes only

Fig.19 indicates O-Xylene selectivity versus time at different temperatures. It is clear that this selectivity is high for higher temperatures, which was predictable due to the fact that high temperatures provide a condition under which the bonds can be broken more easily and since O-Xylene is a lighter product of the reaction compared to n-propylbenzene and 2-ethyltoluene, its selectivity would go up at higher temperatures. This trend is in agreement with literature [29] which reported that the ring opening conversion would go up by increasing the temperature but it also mentioned that these products are poor from a cetane number point of view. On the other hand, due to deactivation of the catalyst

during the reaction, this selectivity decreased and this trend was sharper for higher temperatures while the trend of conversion was smoother at higher temperatures, which could imply that despite the fact that the catalyst is more stable at higher temperatures, it would lose its activity faster at higher temperatures resulting in upward trend for n-propylbenzene and 2-ethyltoluene.

At 350°C and 360°C the selectivity of 2-ethyltoluene is mostly higher than 50%, which indicates that the major product of the reaction is 2-Ethyltoluene implying that β scissoring (the product is 2-Ethyltoluene) is easier than α scissoring (the product is n-propylbenzene).

Fig.22. Desired products yield at different temperatures versus Time on Stream (min)
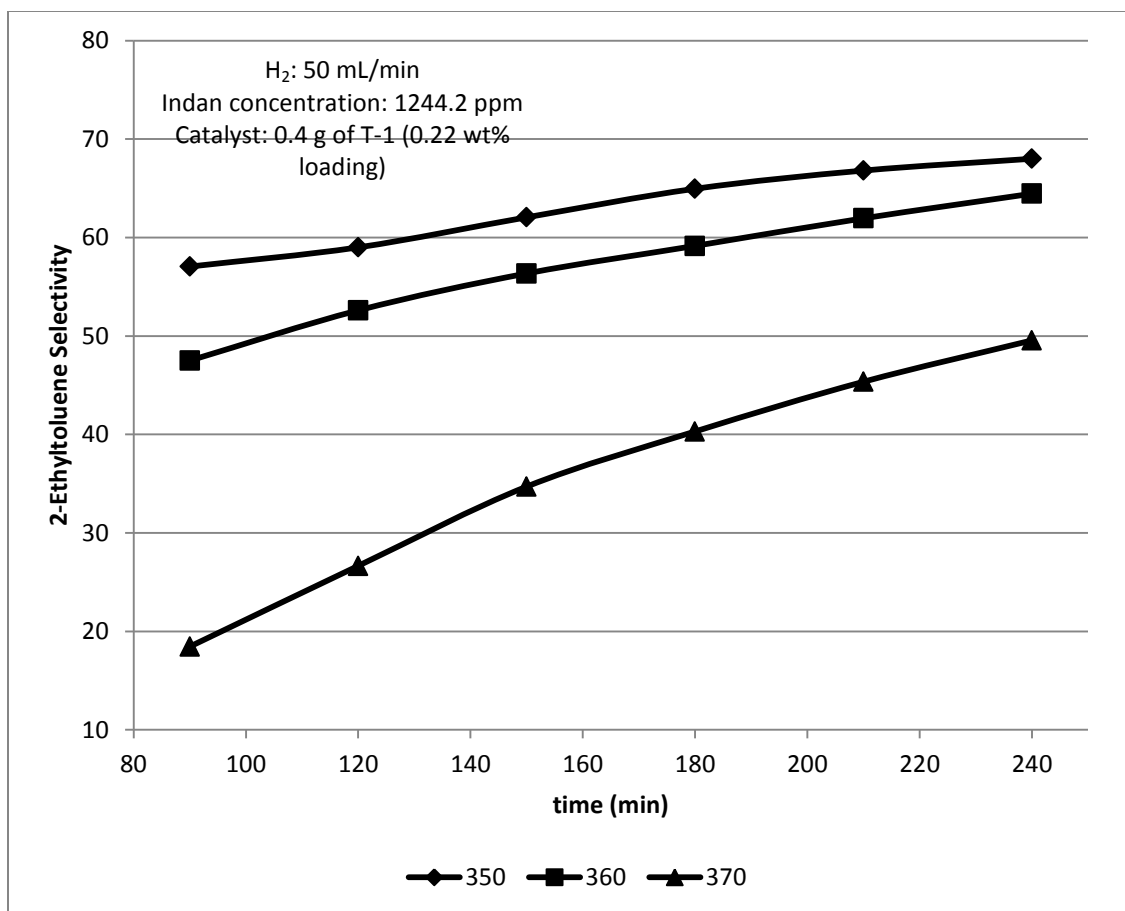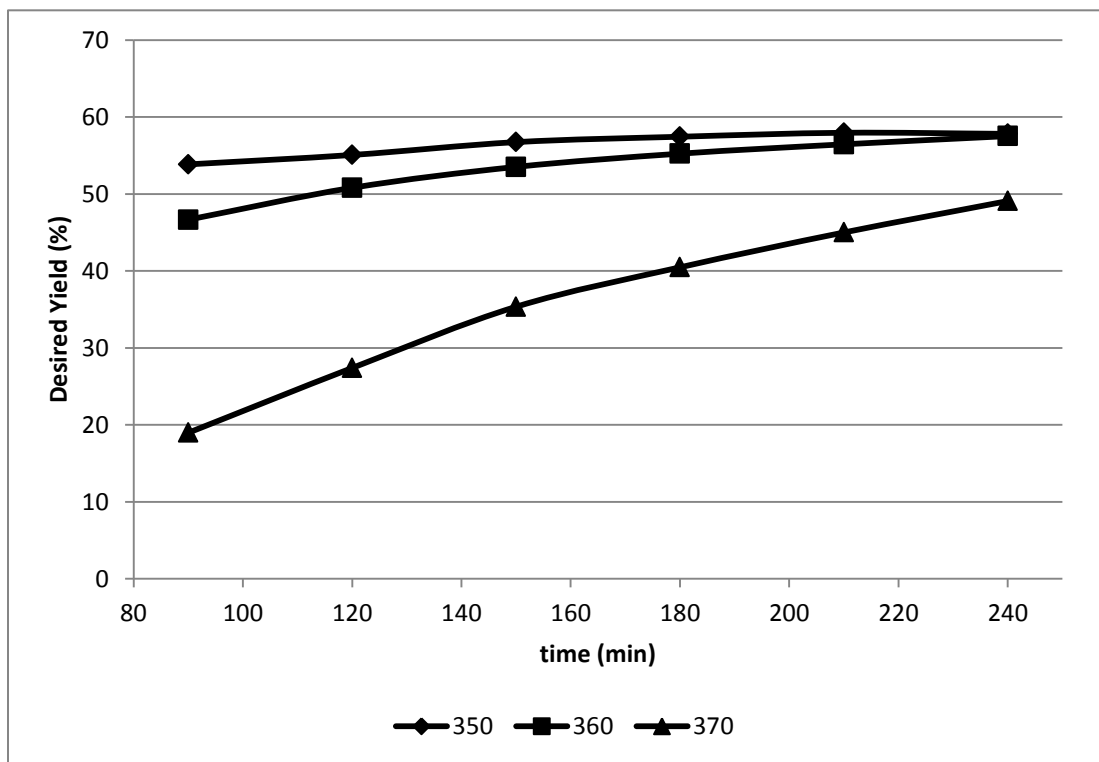The lines between data points are to guide eyes only

The desired products are the ones with unaffected carbon atom amount (n-Propylbenzene and 2-Ethyltoluene), among which 2-propylbenzene is preferable for the cetane number increase. At lower temperatures and partially deactivated catalyst higher selectivity can be achieved. On the other hand, lower temperatures lead to lower conversions, so the optimal temperature choice should be based on the product yield (yield= selectivity X conversion), which is shown in Fig.22.

From the graphs and data shown above, it is clear that 350°C gives us more yield of desired products (n-propylbenzene and 2-ethyltoluene) while at higher temperatures, the conversion is higher but the products of the reaction shift from the compounds of high cetane number to compounds of low cetane number. This is consistent with the findings of Nylen et al. [28] (they reported 325°C as the temperature to achieve the highest cetane number and increasing the temperature from that point reduces the cetane number of products at 220 bar).

To further study the influence of temperature on the indan RO reaction using Ir on porous γ- Al_2O_3, a set of experiments were done in a differential reactor to calculate the activation energy of indan RO. The catalyst used in these experiments had 0.23 wt.% Ir loading and a total amount of 0.27 g catalyst was used in each reaction (the hydrogen flow rate was 120 mL/min). The conversions

71

for 350°C, 360°C, 370°C and 380°C was 8.32%, 11.16%, 13.65% and 16.84% respectively. The graph below shows the Ln (conversion) versus 1/T; based on the slope, the activation energy was found as 78kJ/mol.

Activation Energy

$$y = -9426.4x + 17.272$$
$$R^2 = 0.9937$$
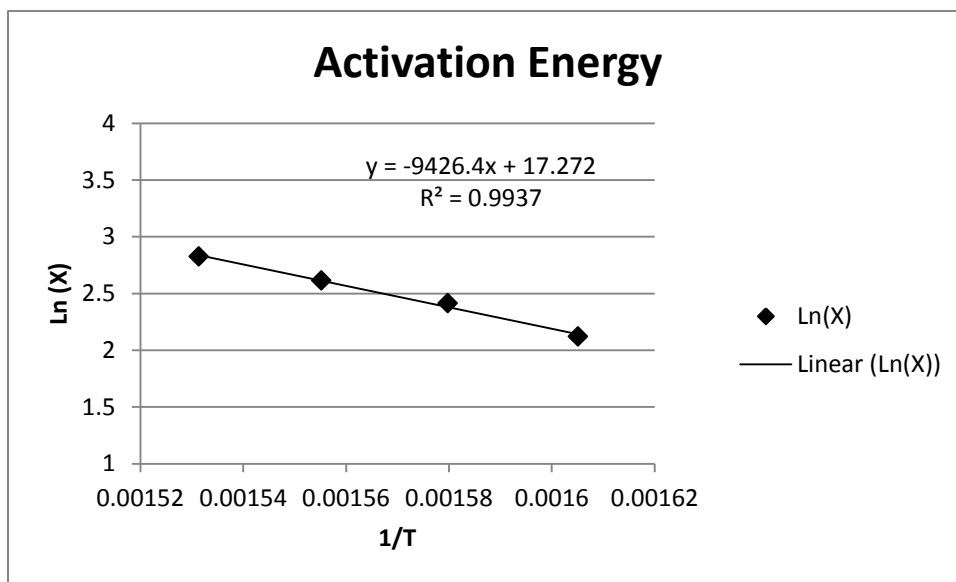
Fig.23. Arrhenius plot for Ir nano particles on powdered γ-alumina : 0.27 g catalyst with 0.23 wt% loading and hydrogen flow rate of 120 mL/min

The difference between this activation energy and the one calculated using Ir/oxidized-SMF is most likely due to the structure of metal nanoparticles deposited on the support. TEM images showed that there are both aggregates (Fig. 24) and individual (Fig. 25) nanoparticles on SMF while on γ- Al_2O_3 there are only individual nanoparticles of ~2 nm [73].
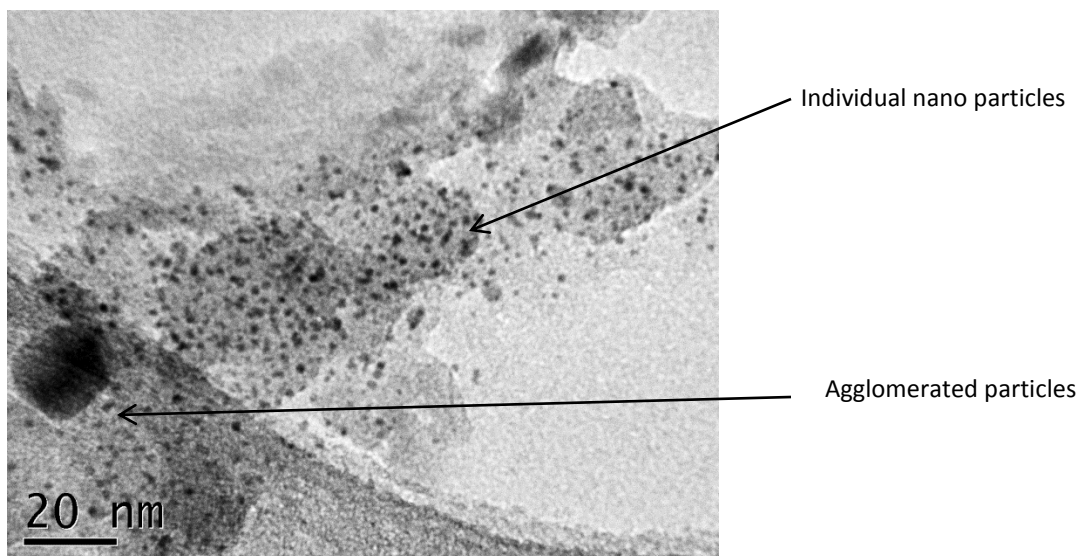
Fig. 24. Aggregates and individual nanoparticles on SMF
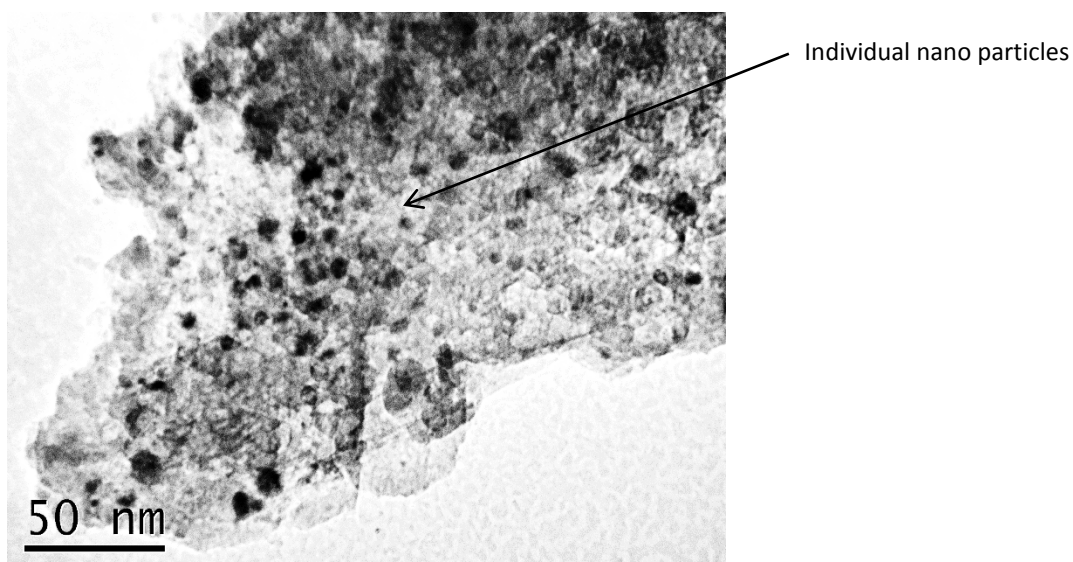
Fig. 25. Individual nanoparticles on SMF

Aggregation can be a cause of different activation energy, as the type of active sites may be different (defect or terrace atoms, or their ensembles). Various active sites of the same metal have different electronic and geometric characteristics resulting in different modes of reactant adsorption and their chemisorption strength, leading to different activation energy [77].

4.3.3. Removal of Ir nanoparticle organic stabilizer

In this thesis, as we aimed to produce a structured ring opening catalyst, only low Ir loadings could be achieved due to the low surface area of the support. As typically known for heterogeneous catalyst preparation, low loadings result in small active metal nanoparticle sizes, which might not be high enough for necessary surface area requirements for the reactant adsorption. That is why the preformed Ir nanoparticles with known RO catalytic activity were deposited as active phase. Steric stabilization was used to produce preformed Ir nanoparticles and this was achieved using a linear polymer PVP, PVP is one of the most used nanoparticle stabilizers and the size of the particles can be controlled by changing the concentration of such a stabilizer (higher concentrations lead to smaller particles). After the synthesis and nanoparticle deposition, the polymer functional groups remain absorbed on the nanoparticles` surface and may interfere with the adsorption of reactants during a catalytic process [81, 82].

Peniche et al. [69] studied the degradation of pure PVP using TGA and FTIR. The reported results indicate that under nitrogen atmosphere, the decomposition temperature range of PVP is 400-450 °C and under oxygen atmosphere, this range changed to 300-550 °C. Also the activation energy for the decomposition reaction was reported to be around 242 kJ/mol under nitrogen and for oxygen

atmosphere, this value changed from 199 kJ/mol in the beginning of the reaction to 306 kJ /mol towards the end of decomposition.

The presence of metal nanoparticles can affect the thermal decomposition of PVP. As investigated by Du et al. [70], the presence of Pt nanoparticles resulted in 28% less decomposition of PVP compared to pure PVP and also the starting temperature of decomposition changed from 380°C (for pure PVP) to 350°C (in the presence of Pt nanoparticles). Among PVP removal techniques, the most effective method according to Song et al. [71] is the oxidation-reduction method. In this procedure, the catalyst with PVP first thermally treated under oxygen atmosphere (air) and then reduced under hydrogen atmosphere which can provide us with a clean catalyst. Thus, a high temperature pretreatment in oxygen followed by hydrogen is recommended to remove the PVP from nanoparticles; the exact conditions depend on the nature of nanoparticles and are not known for PVP-Ir composites. Below, we report our study on the PVP removal from Ir nanoparticles deposited on the powdered support.

This study was performed with the help of TGA device. All of the experiments in this section had a step of moisture vaporization in which the samples were heated up to 100°C with the highest ramp (50°C/min) and kept at that temperature for 20 minutes.
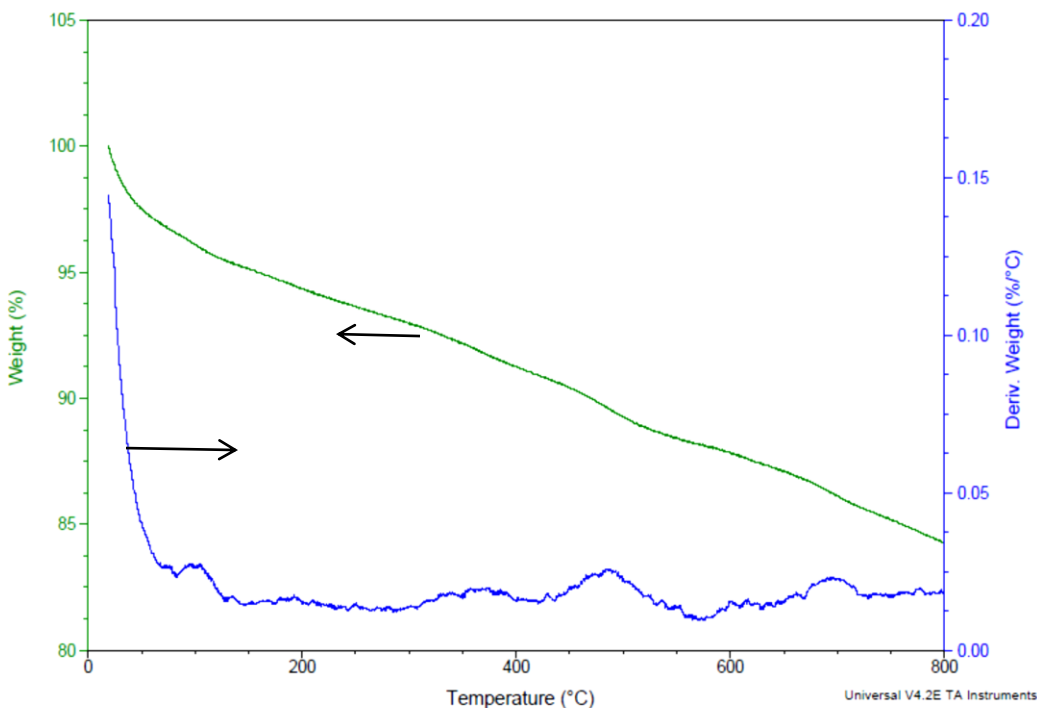
Fig.26.Sample A-1, No pre-treatment
TGA condition: N2 atmosphere, ramp 5°C/min from 25°C to 800°C

Fig.26 shows the weight change during the TGA run for sample A-1 in nitrogen atmosphere. This sample is the fresh untreated Ir/ɣ-Al$_2$O$_3$ (0.22 wt.% Ir, 3.5 wt.% PVP). The final weight after the TGA for this sample is 84%, so 16% of the sample mass was lost and this amount can be attributed mostly to PVP used during sample preparation. This mass loss is almost at a constant rate (0.02) so there is not any kind of reaction occurring at a certain temperature (this was predictable as the purge gas is inert) except 500°C, at which we can see an increase in mass loss due to decomposition of PVP to mostly pyrrolidone [67]. This decomposition is probably the decomposition of products of an initial decomposition, which

occurs at 350-380°C without mass loss due to the fact that a polymer usually

decomposes to its units (PVP decomposition).
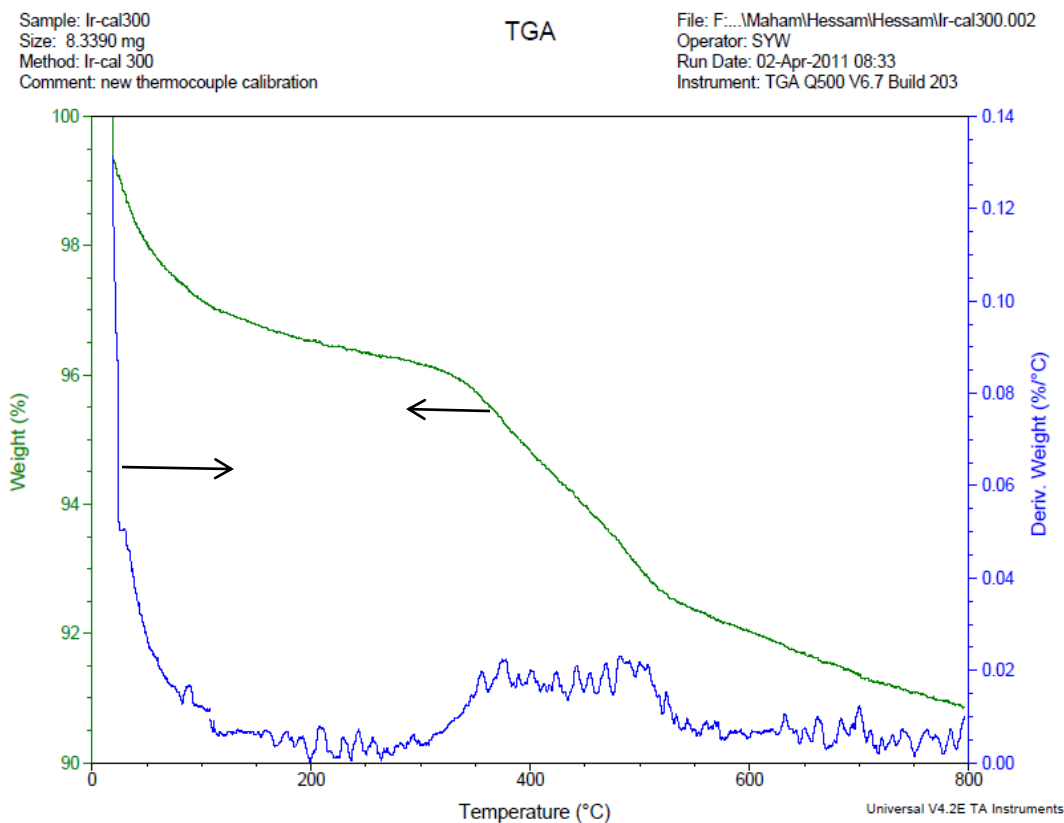
Fig.27.Sample A-2, Calcined at 300°C for 1 hour
TGA condition: N2 atmosphere, ramp 5°C/min from 25°C to 800°C

Fig.27 is a result of thermo gravitational analysis of the A-2 sample, which has

the same conditions as A-1 (0.22 wt.% Ir and 3.5 wt.% PVP before calcination)

but was previously calcined in air at 300°C for 1 hour. We can see sudden mass

loss at the beginning of the process, similar to the A-1 sample. The mass loss

trend is almost smooth and constant for the rest of the graph and the final mass

is almost 91%, which indicates a 9% mass loss. The decomposition of products of

PVP decomposition can also be seen in this graph around 550°C, which is consistent with A-1 graph.

Universal V4.2E TA Instruments
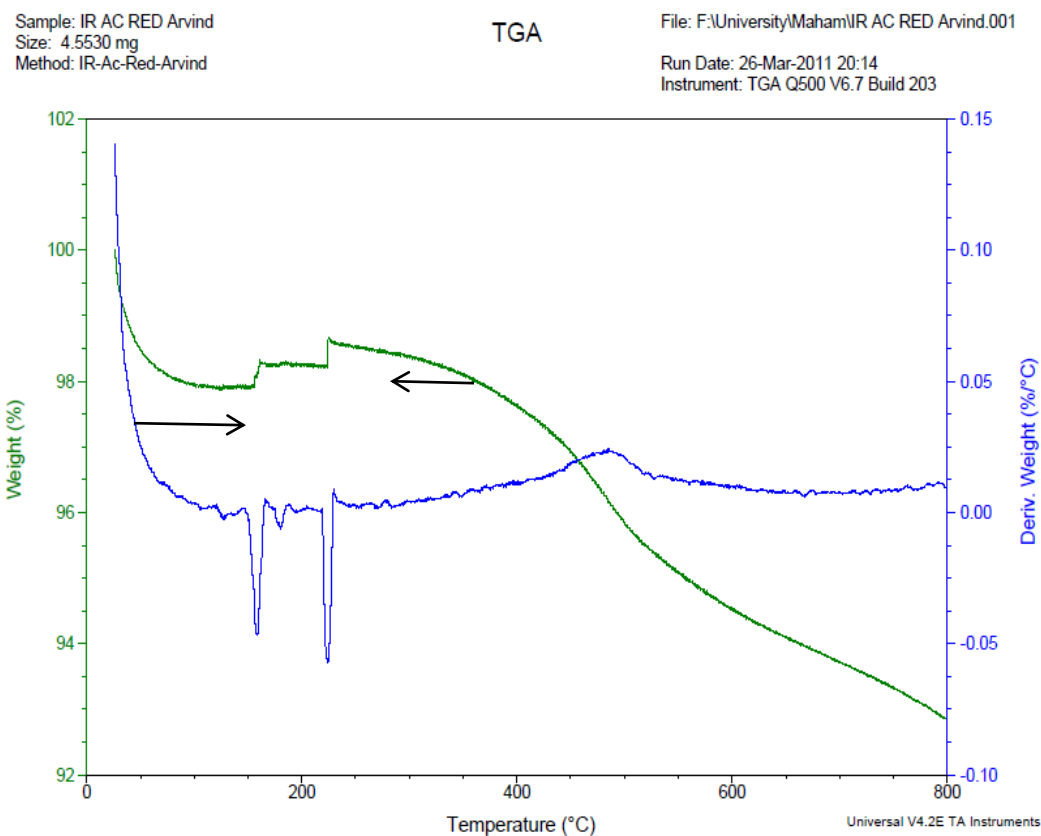
Fig.28.Sample: A-3, Calcined at 300°C for 1 hour and reduced at 300°C for 1 hour under H2 atmosphere
TGA condition: N2 atmosphere, ramp 5°C/min from 25°C to 800°C

Fig.28 is for the last sample (A-3), which is basically the A-1 sample (0.22 wt.% Ir and 3.5 wt.% PVP before calcination) but calcined at 300°C for 1 hour and reduced under hydrogen atmosphere (80 mL/min) at 375°C in a tubular reactor. The final mass is 93%, which implies a mass loss of 7%. The graph shows a 2 step physisorption occurring at 150°C and 200°C and again we can see decomposition at 500°C. If we deduct the physisorption from the overall mass loss, the mass

loss would be less than 6%, which indicates that reduction had a small effect on removing the PVP.
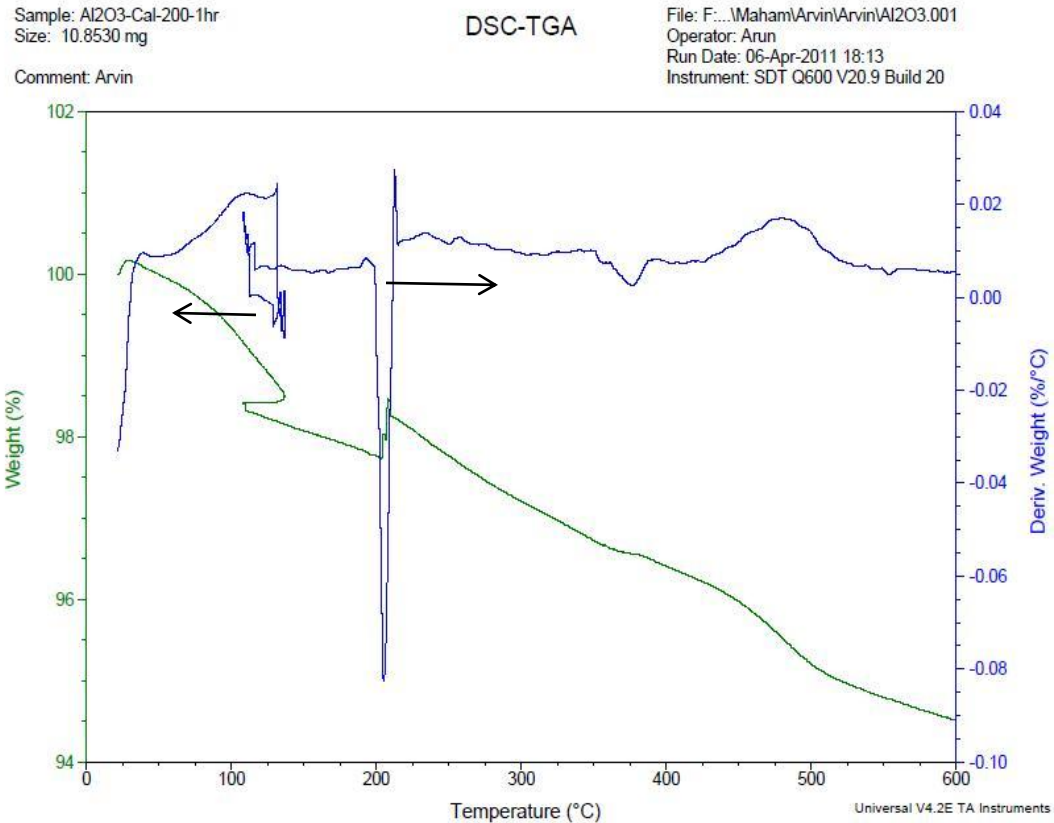
Fig.29.Sample: Pure Alumina
TGA condition: N2 atmosphere, ramp 5°C/min from 25°C to 600°C

As a control experiment, TGA of the pure alumina was performed as well. As Fig.29 shows, the alumina itself has almost 5% mass loss and also we can see that the physisorption has occurred here again at 200°C, which explains the mass gains for the A-3 sample at the same temperature. This amount of mass loss is the support mass loss (without PVP) so if we deduct this mass loss from all of the results, and also if we consider the mass losses under 200°C as a result of surface water [67], we can understand that the amount of PVP remaining in the samples

after calcination and reduction is not considerable. The amount of mass loss before calcination was (16-5=11%) and after calcination plus reduction this value dropped to (7-5=2%). These amounts indicate almost 81% removal of PVP. In ideal cases, the PVP and other undesired organic compounds should be removed 100% from the catalyst in order for the reactants to use the surface of the active phase without any obstruction since these obstructions can lead to lower observed activity of the catalyst. This obstruction can also affect the selectivity. The catalyst showed a higher selectivity in lower activities but this contrast was not in favour of the yield (leading to lower yield) which is the main important factor.

As a conclusion, the pretreatment of PVP-stabilized Ir nanoparticles at 300°C for 1 hour in air followed by a hydrogen treatment for 1 hour at 375°C showed the best removal of PVP stabilizer and its removal efficiency was almost 81%.

Chapter 5. Conclusion

Nanostructured iridium nanoparticles and structured sintered metal microfibers (SMF) were investigated as an active phase and a support, respectively, in ring opening of a model compound, indan, to estimate the material's suitability for further studies in oil refining processes. The SMF was oxidized through a three-step process which allowed alumina whiskers of 200 nm to grow on the surface of metal fibers. A synthesized NiMo/SMF catalyst (3 wt.% Ni, 12 wt.% Mo) required impractically high catalyst amounts to achieve reasonable conversions in indan hydrotreatment, and it was not mechanically stable. Iridium nanoparticles were further selected as suitable active phase as Ir is the most active metal for indan ring opening. 0.125 wt.% Ir/SMF showed practical conversion in indan ring opening. The Ir/SMF material allowed absence of external mass transfer limitations, and the nanoparticles were deposited on the external SMF panel fibers eliminating the internal mass transfer as well. The reaction activation energy value was found to be 34 kJ/mol for Ir/SMF while this number was 78 kJ/mol using powdered γ-Al_2O_3 as support. The TEM images revealed that this difference in activation energy could be due to Ir nanoparticle structures. For the γ-Al_2O_3, Ir nanoparticles did not agglomerate but on α-Al_2O_3 (SMF surface) the particles could be seen both in individual form and aggregated form. Characterization on SMF illustrated that high ratio of fibers` diameter to

whiskers height, could be a cause of not achieving high loadings because most of the volume is occupied by the metal fiber itself which surface is not accessible but on the other hand, this matter is a great asset towards removing mass and heat transfer limitations. Also dispersion of active metal on SMF was observed to be mainly on the surface hence the deeper layers of SMF could not be used. The probable causes of this phenomenon can be drainage of the precursor solution from the mid layers of SMF or fast evaporation of the precursor solution, both leading to higher concentration of nanoparticles at the surface of the SMF.

The thermal behaviour studies at 350°C, 360°C and 370°C using Ir on powdered γ-Al$_2$O$_3$ showed that lower temperatures (350°C) would lead to higher yield of desired products due to lower selectivity to light products, which do not fall under the category of desired products. The pretreatment of PVP-stabilized Ir nanoparticles at 300°C for 1 hour in air followed by a hydrogen treatment for 1 hour at 375°C showed the best removal of PVP stabilizer and its removal efficiency was almost 81%. The presence of PVP would result in reducing the surface area of the active metal available for the ring opening reaction.

This study may pave the way to the development of structured catalysts with enhanced mass and heat transfer limitations for fast catalytic reactions requiring low loading of catalytically active phase such as cases of polymer production

during which low catalyst loading is required to achieve high molecular weight

materials [84].

Chapter 6. Future work

Further investigation to understand the benefits and setbacks of such structured catalyst, which mentioned in this thesis, can be a reasonable future work for this study. A comparative catalyst deactivation study between introduced structure and conventional structures can be performed. The structured support should be more developed (from a material point of view) to allow more loading of active phase to be deposited in order to achieve better results and compete with other supports. This can be achieved by making the support less compact or by making the fibers porous which leads to having more surface for active phase to be deposited. Also other causes of getting low loadings such as drainage or fast evaporation of precursor (from mid layers of SMF) can be further investigated. On the other hand, this material can be used in other industries such as piping to improve pressure drop since Ox-SMF is hydrophobic. RO kinetic studies should be performed, followed by kinetic modeling to find the intrinsic rate constants and adsorption constants.

The thermal behaviour of ring opening won`t change identically between different temperatures; therefore this can be an area of interest for further studies and better understanding about temperature dependency of indan ring opening.

References

[1] Cybulski A.; Moulijn J.A. *Structured Catalysts and Reactors*, 2nd ed.; CRC Press: 2005; pp 1-14, 579-583.

[2] Ettaz Samad J. Oxidation Synthesis and Reaction Analysis of a New Arranged Catalyst Support. M.Sc. Thesis, University of Alberta, Edmonton, AB, 2010.

[3] Furimsky E. *Catalyst for Upgrading Heavy Petroleum Feeds: Studies in Surface Science and Catalysis*; Elsevier: 2007; Vol. 169, pp 1-4, 43-47.

[4] *Proposal for a Directive of the European Parliament and of the Council on the quality of petrol and diesel fuels and amending*; Directive 98/70/EC; Commission of the European Communities; Brussels, 2001.

[5] *Tier 2 Motor Vehicle Emission Standards and Gasoline Sulfur Control Requirements;* EPA420-R-99-024; United States Environmental Protection Agency: 1999.

[6] Venner S.F. EU Environmental Laws Impact Fuels' Requirements, *Hydrocarbon processing*. **2000**, *79,* 51-54.

[7] Parkinson G.; Crabb C.; Enright A.; Kamiya T.; Ondrey G. Refining - Refiners Ride a Rough Road, *Chemical Engineering*. **1999**, *106*, 483-485.

[8] Ma X.; Sakanishi K.; Mochida I. Hydrodesulfurization Reactivities of Various Sulfur Compounds in Diesel Fuel, *Industrial Chemistry and Engineering Research.* **1994**, 33, 218-222.

[9] Kilanowski D.R.; Teeuwen H.; de Beer V.H.J.; Gates B.C.; Schuit G.C.A.; Kwart H. Hydrodesulfurization of Thiophene, Benzothiophene, Dibenzothiophene, and Related Compounds Catalyzed by Sulfided $CoO-MoO_3/ɣ-Al_2O_3$: Low-pressure Reactivity Studies, *Journal of catalysis*. **1978**, *55,* 129-137.

[10] Shih, S.S; Ketzer, J.R.; Kwart, Preprints of ACS division of Petroleum Chemistry, Vol. 22 (1977), 919.

[11] Ledoux M.J.; Huu C.P.; Segura Y. S. Correlation between Low-Pressure Thiophene HDS and High-Pressure Dibenzothiophene HDS, *Journal of Catalysis*. **1990**, *21*, 70-76.

[12] Eliezer F.K.; Bhinde M.; Houalla M.; Broderick D.; Gates B.C.; Katzer J.R.; Olson J.H. A Flow Microreactor for Study of High-Pressure Catalytic

Hydroprocessing Reactions, *Industrial & Engineering Chemistry Fundamentals*. **1977**, *16*, 380-384.

[13] Sporka K.; Hanika J. Development of Cobalt-Molybdenum Hydrodesulfurization Catalysts, *Collection of Czechoslovak Chemical Community*, **1992**, *57*, 2501-2508.

[14] Shi L.; Tin K.C.; Wong N.B.; Li C.L. Hydrodesulfurization Of Petroleum Components, *Petroleum Science and Technology*, **1999**, *17*, 519-533.

[15] Babich I.V.; Moulijn J.A. Science and Technology of Novel Processes for Deep Desulfurization of Oil Refinery Streams: a Review, *Fuel*, **2003**, *82*, 607-631.

[16] Vander Linde B.; Menon R.; Dave D.; Gustas S. SynTechnology: an Attractive Solution for Meeting Future Diesel Specifications, in: Presented at the Asian Refining Technology Conference, ARTC, 1999.

[17] Langston J.; Allen L.; Dave´ D. Technologies to achieve 2000 diesel specifications, *Petroleum Technology Quarterly.* **1999**, 65-70.

[18] Furimsky E.; Massoth F.E. Hydrodenitrogenation of Petroleum, *Catalysis Reviews: Science & Engineering.* **2005**, *47*, 297-489.

[19] Yang M.; Grange P.; Delmon B. Secondary Effect of Hydrogen Sulfide on HDN Reaction, *Applied Catalysis A: General*. **1997**, *154*, L7-L15.

[20] Gualda G.; Kasztelan S. Initial Deactivation of Residue Hydrodemetallization Catalysts, *Journal of Catalysis.* **1996**, *161*, 319-337.

[21] Weisz P.B.; Prater C.D. Interpretation of Measurements in Experimental Catalysis, *Advances in Catalysis*. **1954**, *6*, 143-196.

[22] Petersen E.E. Chemical Reaction Analysis, *AIChe Journal*. **1965**, *11*, 770-955.

[23] Himmelblau D.M.; Jones C.R.; Bischoff K.B. Determination of Rate Constants for Complex Kinetics Models, *Industrial & Engineering Chemistry Fundamentals*. **1967**, *6*, 539-543.

[24] Madon R.M.; Boudart M. Experimental Criterion for the Absence of Artifacts in the Measurement of Rates of Heterogeneous Catalytic Reactions, *Industrial & Engineering Chemistry Fundamentals*. **1982**, *21*, 438-447.

[25] Koros R.M.; Nowak E.J. A Diagnostic Test of the Kinetic Regime in a Packed Bed Reactor, *Chemical Engineering Science*. **1967**, *22*, 470.

[26] Vannice M.A. *Kinetics of Catalytic Reactions*; Springer Science: 2005; pp 77-82.

[27] Finlayson B.A. University of Washington Faculty Webserver. (accessed July 2012)

http://faculty.washington.edu/finlayso/ebook/reaction/rxndiff/nondim.htm

[28] Nylen U.; Sassu L.; Melis S.; Jaras S.; Boutonnet M. Catalytic Ring Opening of Naphthenic Structures Part I. From Laboratory Catalyst Screening via Pilot Unit Testing to Industrial Application for Upgrading LCO into a High-quality Diesel-blending Component, *Applied Catalysis A: General*. **2006**, *299,* 1-13.

[29] Nylen U.; Delgado J.F.; Jaras S.; Boutonnet M. Low and High-pressure Ring Opening of Indan over 2 wt % Pt, Ir and bi-metallic $Pt_{25}Ir_{75}$/boehmite Catalysts Prepared from Microemulsion Systems, *Applied Catalysis A: General*. **2004**, *262*, 189-200.

[30] Davidova N.P.; Penchev V.Zh. Conversion of Alkylaromatic Hydrocarbons over a Nickel-Zeolite Catalyst, *Collection of Czechoslovak Chemical Community*. **1975**, *40*, 1901-1909.

[31] Guidot G.; Germain J.E. Hydrogenolysis and Isomerization of Indan on Metallic Catalysts, *Annales de Chimie*. **1974**, *9*, 191-201.

[32] Frety R.; Da Silva P.N.; Guenin M. Supported Iridium Catalysts: Comparison between Resistance to Sulphur Poisoning and Hydrodesulphurization Properties, *Applied Catalysis*. **1990**, *57*, 99-103.

[33] Lin T.B.; Jan C.A.; Chang J.R. Aromatics Reduction over Supported Platinum Catalysts: Improvement in Sulfur Resistance by Addition of Palladium to Supported Platinum Catalysts, *Industrial & Engineering Chemistry Research*. **1995**, *34*, 4284-4289.

 [34] Wikipedia the Free Encyclopedia. http://en.wikipedia.org/wiki/Monolith (accessed July 2012).

[35] Nijhuis T.A.; Kreutzer M.T.; Romijn A.C.J.; Kapteijn F.; Moulijn J.A. Monolithic Catalysts as Efficient Three-phase Reactors, *Chemical Engineering Science*. **2001**, *56*, 823-829.

[36] Smits H.A.; Stankiewicz A.; Glasz W.C. Selective Three-phase Hydrogenation of Unsaturated Hydrocarbons in a Monolithic Reactor, *Chemical Engineering Science*. **1996**, *51*, 3019-3025.

[37] Asik J.; Meyer G.; Dobson D. Lean NOx Trap Desulfation Through Rapid Air Fuel Modulation, SAE Technical Paper (2000), # 2000-01-1200.

[38] Iwachido K.; Tanada H.; Watanabe T.; Yamada N.; Nakayama O.; Ando H.; Hori M.; Taniguchi S.; Noda N.; Abe F. Development of the NOx Adsorber Catalyst for Use with High-Temperature Condition, SAE Technical Paper (2001), # 2001-01-1298.

[39] Kojima S.; Baba N.; Matsunaga S.I.; Senda K.; Katoh K.; Itoh T. Modeling and Numerical Analysis of NOx Storage-Reduction Catalysts - On the Two Effects of Rich-Spike Duration, SAE Technical Paper (2001), # 2001-01-1297.

[40] Sanchez Marcano G.J.; Tsotsis T.T. *Catalytic Membranes and Membrane Reactors*; Wiley-VCH Verlag GmbH: 2002.

[41] Collins J.P.; Way J. D. Catalytic Decomposition of Ammonia in a Membrane Reactor, *Journal of Membrane Science*, **1994**, *96*, 259-274.

[42] Matatov-Meytal Y.; Sheintuch M. Catalytic Fibers and Cloths, *Applied Catalysis A: General.* **2002**, *231*, 1-16.

[43] Plourde M.; Belkacemi K.; Arul J. Hydrogenation of Sunflower Oil with Novel Pd Catalysts Supported on Structured Silica, *Industrial and Engineering Chemistry Research*. **2004***, 43*, 2382-2390.

[44] Tribolet P.; Kiwi-Minsker L. Palladium on Carbon Nano Fibers Grown on Metallic Filters as Novel Structured Catalyst, *Catalysis Today.* **2005**, *105*, 337-343.

[45] Semagina N.; Grasemann M.; Xanthopoulos N.; Renken A.; Kiwi-Minsker L. Structured Catalyst of Pd/ZnO on Sintered Metal Fibers for 2-Methyl-3-Butyn-2-ol Selective Hydrogenation, *Journal of Catalysis*. **2007**, *251*, 213-222.

[46] Samad J.E.; Nychka J.A.; Semagina N.V. Structured Catalysts via Multiple Stage Thermal Oxidation Synthesis of FeCrAl Alloy Sintered Microfibers, *Chemical Engineering Journal*. **2011**, *168*, 470-476.

[47] Brown K.R.; Walter D.G.; Natan M.J. Seeding of Colloidal Au Nanoparticle Solutions. 2. Improved Control of Particle Size and Shape, *Chemistry of Materials*. **2000**, *12*, 306-313.

[48] Chen D.H.; Yeh J.J.; Huang T.C. Synthesis of Platinum Ultrafine Particles in AOT Reverse Micelles, *Journal of Colloid and Interface Science*. **1999**, *215*, 159-166.

[49] Devarajan S.; Bera P.; Sampath S. Bimetallic Nanoparticles: A Single Step Synthesis, Stabilization, and Characterization of Au–Ag, Au–Pd, and Au–Pt in sol–gel Derived Silicates, *Journal of Colloid and Interface Science*. **2005**, *290*, 117-129.

[50] Hostetler M. J.; Wingate J. E.; Zhong C. J.; Harris J. E.; Vachet R. W.; Clark M. R.; Londono J. D.; Green J. S.; Stokes J. J.; Wignall G. D.; Glish G. L.; Porter M. D.; Evans N. D.; Murray R. W. Alkanethiolate Gold Cluster Molecules with Core Diameters from 1.5 to 5.2 nm: Core and Monolayer Properties as a Function of Core Size, *Langmuir*. **1998**, *14*, 17-30.

[51] Watzky M. A.; Finke R. G. Nanocluster Size-Control and "Magic Number" Investigations. Experimental Tests of the "Living-Metal Polymer" Concept and of Mechanism-Based Size-Control Predictions Leading to the Syntheses of iridium (0) Nanoclusters Centering about Four Sequential Magic Numbers, *Chemistry of Materials*. **1997**, *9*, 3083-3095.

[52] Brown K. R.; Natan M. J. Hydroxylamine Seeding of Colloidal Au Nanoparticles in Solution and on Surfaces, *Langmuir*. **1998**, *14*, 726-728.

[53] Henglein A.; Giersig M. Formation of Colloidal Silver Nanoparticles: Capping Action of Citrate, *Journal of Physical Chemistry*. **1999**, *103*, 9533-9539.

[54] Teranishi T.; Hosoe M.; Tanaka T.; Miyake M. Size Control of Monodispersed Pt Nanoparticles and Their 2D Organization by Electrophoretic Deposition, *Journal of Physical Chemistry*. **1999**, *103*, 3818-3827.

[55] Chen Y.; Liew K. Y.; Li J. Size-controlled Synthesis of Ru Nanoparticles by Ethylene Glycol Eeduction, *Materials Letters*. **2008**, *62*, 1018-1021.

[56] Yan X.; Liu H.; Liew K. Y. Size Control of Polymer-Stabilized Ruthenium Nanoparticles by Polyol Reduction, *Journal of Materials Chemistry.* **2001**, *11*, 3387-3391.

[57] Teranishi T.; Miyake M. Size Control of Palladium Nanoparticles and Their Crystal Structures, *Chemistry of Materials*. **1998**, *10*, 594-600.

[58] The A to Z of the Materials; http://www.azom.com/article.aspx?ArticleID=1389 (accessed July 2012).

[59] Pecchi G.; Reyes P.; Lopez T.; Gomez R. Pd-CeO2 and Pd-La2O3/Alumina-Supported Catalysts: Their Effect on the Catalytic Combustion of Methane, *Journal of Non-Crystalline Solids*. **2004**, *345* & *346*, 624-627.

[60] Marquez-Alvarez C.; Zilkova N.; Perez-Pariente J.; Cejka J. Synthesis, Characterization and Catalytic Applications of Organized Mesoporous Aluminas, *Catalysis Reviews*. **2008**, *50*, 222-286.

[61] Kaluza L.; Zdrazil M.; Zilkova N.; Cejka J. High Activity of Highly Loaded MoS$_2$ Hydrodesulfurization Catalysts Supported on Organized Mesoporous Alumina, *Catalysis Communications*. **2002**, *3*, 151-157.

[62] Kim P.; Kim Y.; Kim H.; Song I.; Yi J. Synthesis and Characterization of Mesoporous Alumina for Use as Catalyst Support in the Hydrodechlorination of 1, 2-Dichloropropane: Effect of Preparation Condition of Mesoporous Alumina, *Journal of Molecular Catalysis A: Chemical*. **2004**, *219*, 87-95.

[63] Valange S.; Berraultt J.; Derouault A.; Gabelica Z. Binary Cu–Al Mesophases Precursors to Uniformly Sized Copper Particles Highly Dispersed on Mesoporous Alumina, *Microporous and Mesoporous Materials.* **2001**, *44 & 45*, 211-220.

[64] Lenarda M.; Moretti E.; Storaro L.; Patrono P.; Pinzan F.; Rodriguez-Castellon E.; Jimenez-Lopez A.; Busca G.; Finocchio E.; Montanari T.; Frattini R. Finely Dispersed Pd-Zn Catalyst Supported on an Organized Mesoporous Alumina for Hydrogen Production by Methanol Steam Reforming, *Applied Catalysis A: General*. **2006**, *312*, 220-228.

[65] Scott Fogler H. *Essentials of Chemical Reaction Engineering, 4th ed.*; Pearson Education Inc.: 2010.

[66] Varma A. Packed Bed Reactors: An Overview, *ACS Symposium Series*. **1981**, *168*, 279-286.

[67] Du Y.K.; Yang P.; Mou Z.G.; Hua N.P.; Jiang L. Thermal Decomposition Behaviour of PVP Coated on Platinum Nanoparticles, *Applied Polymer Science*. **2006**, *99*, 23-26.

[68] Richardson J.F.; Peacock D.G. *Coulson and Richardson`s Chemical Engineering: Chemical and Biochemical Reactors and Process Control*, 3rd ed.; Elsevier Ltd: 1994; Vol. 3, pp. 112-113.

[69] Peniche C.; Zaldivar D.; Pazis M.; Paz S.; Bullay A.; San Roman J. Study of the Thermal Degradation of Poly (N-vinyl-2-pyrrolidone) by Thermogravimetry-FTIR, *Journal of Applied Polymer Science.* **1993**, *50*, 485-493.

[70] Du Y. K.; Yang P.; Mou Z. G.; Hua N. P.; Jiang L. Thermal Decomposition Behaviors of PVP Coated on Platinum Nanoparticles, *Journal of Applied Polymer Science*. **2006**, *99*, 23-26.

[71] Song H.; Rioux R. M.; Hoefelmeyer J. D.; Komor R.; Niesz K.; Grass M.; Yang P.; Somorjai G. A. Hydrothermal Growth of Mesoporous SBA-15 Silica in the Presence of PVP-Stabilized Pt Nanoparticles: Synthesis, *Journal of the American Chemical Society*. **2006**, *128*, 3027-3037.

[72] Cheng E. *Arranged Catalysts for Structured Hydrotreating Reactors: Technical report;* WKEXP 905 assignment; University of Alberta; Edmonton, AB, 2011.

[73] Shen J. Bimetallic Catalysts for Low Pressure Ring Opening. M.Sc. Thesis; University of Alberta; Edmonton, AB, 2011.

[74] Blue R. W.; Engle C. J. Hydrogen Transfer over Silica-Alumina Catalysts, *Industrial and Engineering Chemistry.* **1951**, *43*, 494-501.

[75] Holm V. C. F.; Blue R. W. Hydrogen-Deuterium Exchange Activity of Silica-Alumina, *Industrial and Engineering Chemistry*. **1951**, *43*, 501-505.

[76] Forzatti P.; Lietti L. Catalyst Deactivation, *Catalysis Today*. **1999**, *52*, 165-181.

[77] Watanabe M.; Kato S., Ishizeki S.; Inomata H.; Smith Jr. R. L. Heavy Oil Upgrading in the Presence of High Density Water: Basic Study, *Journal of Supercritical Fluids*. **2010**, *53*, 48-52.

[78] Rana M. S.; Samano V.; Ancheyta J.; Diaz J. A. I. A Review of Recent Advances on Process Technologies for Upgrading of Heavy Oils and Residua, *Fuel*. **2007**, *86*, 1216-1231.

[79] Liu Y., Gao L., Wen L., Zong B. Recent Advances in Heavy Oil Hydroprocessing Technologies, *Recent Patents on Chemical Engineering*. **2009**, *2*, 22-36.

[80] Zhang S.; Liu D.; Deng W.; Que G. A Review of Slurry-Phase Hydrocracking Heavy Oil Technology, *Energy Fuels*. **2007**, *21*, 3057

[81] Dartigues J. M.; Chambellan A.; Gault F. G. Isomerization on Metals: Correlation Between Metal Particle Size and Reaction Mechanisms, *Journal of The American Chemical Society*. **1976**, 98, 856-857.

[82] Gonzalez-Cortes S. L.; Dorkjampa S.; Do T. P.; Li Z.; Ramallo-Lopez J. M.; Requejo F. G. Tuning The Ring-Opening Reaction of 1,3-dimethylcyclohexane With The Addition of Potassium Over Ir-Containing Catalysts, Chemical Engineering *Journal*. **2008**, 139, 147-156.

[83] Sanderson R. T. *Chemical Bonds and Bond Energy*, 2nd ed.; Academic Press: 1976.

[84] Radano C. P.; Scherman O. A.; Stingelin-Stutzmann N.; Muller C.; Breiby D. W.; Smith P.; Janssen R. A. J.; Meijer E. A. Crystalline-Crystalline Block Copolymers of Regioregular Poly (3-hexylthiophene) and Polyethylene by Ring-Opening Metathesis Polymerization, *Journal of the American Chemical Society.* **2005**, 127, 12502-12503.